INORGANIC CHEMISTRY
FRONTIERS

RESEARCH ARTICLE

View Article Online
View Journal | View Issue

Check for updates

Cite this: *Inorg. Chem. Front.*, 2024, **11**, 8510

Revealing the effect of host–guest complementarity in supramolecular monofunctional platinum(II) drugs†

Shib Shankar Paul, [a,b] Jan Novotný, [a,b,c]* Jakub Jakubec,[a,b] Kateřina Petrláková,[d] Pia Jurček, [a] Klára Rašková,[a] Michaela Kuchynka, [b,e] Michal Masařík, [d,f] Petr Kulhánek [c] and Radek Marek [a,b,c]*

Monofunctional platinum(II) compounds bearing planar aromatic ligands can be significantly more potent for the treatment of tumors than the traditional bifunctional platinum(II) systems derived from cisplatin. Their properties can be modulated by using a drug carrier, for example, by trapping them into a macrocyclic cavitand and releasing the metallodrug in a controlled manner. In this work, we introduce new monofunctional platinum(II) compounds with the general structure *cis*-$[Pt^{II}(NH_3)_2Cl(4\text{-R-py})]^+NO_3^-$ as direct analogs of pyriplatin, *cis*-$[Pt^{II}(NH_3)_2Cl(py)]^+$. We investigated their chemical activation by aquation in host–guest (HG) complexes with the cucurbit[7]uril (CB7) macrocycle. We used a range of NMR techniques to characterize the HG complexation in detail, and the effects of the ligand on the structure and aquation of chloride at the platinum center in the HG complexes were rationalized with the support of molecular dynamics (MD) simulations and density-functional theory (DFT) calculations. Biological screening of the cytotoxicity and the drug uptake by cell lines A2780 and A2780/CP showed that the cytotoxicity of the Pt-compound with 4-phenylpyridine and 4-pentafluorophenylpyridine ligand was comparable to that of cisplatin and that the cytotoxicity and drug uptake of the Pt-compound with a 4-(1-adamantyl) pyridine ligand was greatly modulated by the CB7 carrier. Our observations indicate great potential for HG complexes in the future supramolecular design and structural tailoring of biological activity.

Received 7th August 2024,
Accepted 22nd October 2024

DOI: 10.1039/d4qi02012j

rsc.li/frontiers-inorganic

Open Access Article. Published on 23 October 2024. Downloaded on 2/12/2026 1:15:43 AM.
This article is licensed under a Creative Commons Attribution 3.0 Unported Licence.

Introduction

The discovery in the 1960s that cancer could be treated with cisplatin revolutionized inorganic medicinal chemistry.[1] Despite the great success of cisplatin, it is not universally effective for all types of cancer[2] and its non-selective mode of action causes a lot of side effects.[3–6] Many types of cancer are either inherently resistant or quickly acquire resistance to cisplatin therapy.[7–11] To overcome these problems, the anticancer properties of novel platinum compounds have been investigated.[12–16] A large number of compounds have been prepared and tested, but only two other platinum drugs (carboplatin[17] and oxaliplatin[18]) have been approved for clinical use worldwide.[19]

Monofunctional platinum(II) compounds represent a class of nonclassical compounds which are designed to form only a single coordination bond with DNA, unlike bifunctional compounds of the cisplatin type.[20–22] Studies of the mechanism of action of oxaliplatin have revealed a role for Organic Cation Transporters (OCTs) in cellular uptake and activity.[23] Later studies demonstrated that pyriplatin (**pyPt**), the monofunctional cationic Pt(II) compound *cis*-$[Pt(NH_3)_2Cl(pyridine)]^+$ (Fig. 1a), was transported efficiently by OCT 1 transporter.[24] Structural analysis of **pyPt**-bound DNA showed RNA polymerase (pol) II stalled at the **pyPt** DNA lesion (Fig. 1d). It was suggested that a larger N-heterocycle could stall the RNA pol II even more efficiently.[25] This led to the discovery of phenanthriplatin (**phenPt**), *cis*-$[Pt(NH_3)_2Cl(phenanthridine)]^+$ (Fig. 1b), which was more cytotoxic than cisplatin in a series of cell lines.[26]

Most anticancer metallodrugs tested to date have had two major drawbacks: (i) dose-limiting toxicity[3,27] and (ii) low

[a]*CEITEC – Central European Institute of Technology, Masaryk University, Kamenice 5, CZ-62500 Brno, Czechia. E-mail: jan.novotny@ceitec.muni.cz, radek.marek@ceitec.muni.cz; https://twitter.com/LabMarek*
[b]*Department of Chemistry, Faculty of Science, Masaryk University, Kamenice 5, CZ-62500 Brno, Czechia*
[c]*National Center for Biomolecular Research, Faculty of Science, Masaryk University, Kamenice 5, CZ-62500 Brno, Czechia*
[d]*Department of Pathological Physiology, Faculty of Medicine, Masaryk University, Kamenice 5, CZ-62500 Brno, Czechia*
[e]*Department of Chemical Drugs, Faculty of Pharmacy, Masaryk University, Palackého třída 1, CZ-61200 Brno, Czechia*
[f]*Department of Physiology, Faculty of Medicine, Masaryk University, Kamenice 5, CZ-62500 Brno, Czechia*

†Electronic supplementary information (ESI) available. CCDC 2371255 (3). For ESI and crystallographic data in CIF or other electronic format see DOI: https://doi.org/10.1039/d4qi02012j

This journal is © the Partner Organisations 2024

Open Access Article. Published on 23 October 2024. Downloaded on 2/12/2026 1:15:43 AM.
This article is licensed under a Creative Commons Attribution 3.0 Unported Licence.

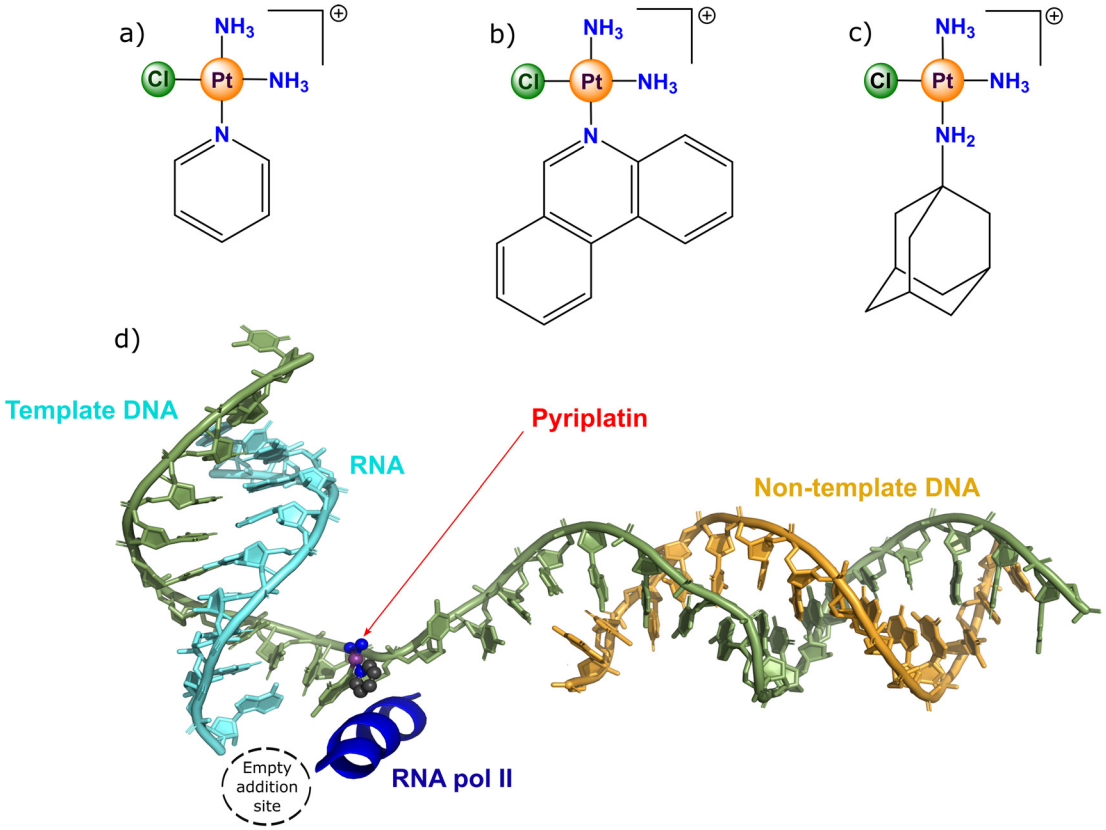

Fig. 1 Structure of (a) pyriplatin (**pyPt**), (b) phenanthriplatin (**phenPt**), (c) adamantylamiplatin (**adaPt**), and (d) X-ray structure of **pyPt**-stalled RNA pol II (generated from PDB: 3M4O according to ref. 25).

selectivity[28] that led to numerous side effects.[29] A solution to the problem could be a drug-carrier system[30,31] designed to protect the Pt-drug from biological nucleophiles during its delivery and to allow site-specific release of the Pt warhead into the tumor tissue.[32–34] An important class of carriers is represented by macrocyclic compounds, such as cucurbit[*n*]urils (CBs) and cyclodextrins (CDs), which are able to form host–guest (HG) inclusion complexes with platinum drugs. In this regard, cisPt has been shown to be completely encapsulated in the cavity of a cucurbit[7]uril (CB7) carrier, but upon aquation of a chloride ligand, the drug translocated towards the CB7 portal.[32] In contrast, oxaliplatin has been shown to be only partially encapsulated in CB7 *via* the hydrophobic cyclohexane moiety.[35] It was later shown that the CB7 container enhanced by a biotin ligand improved the targeted delivery of oxaliplatin into tumor cells.[36] Advances in platinum(II)-based supramolecules have been summarized in several review articles, to which we refer the interested reader.[30,34,37,38]

We previously reported the development of *cis*-$[Pt(NH_3)_2Cl(1\text{-adamantylamine})]^+[NO_3]^-$ (**adaPt**, Fig. 1c) combined with macrocyclic carriers, where we observed the aquation of chloride at the Pt(II) core induced by the CB7 macrocycle, leading to strong HG interaction and the sticking of the active metallodrug in the carrier.[39] The blocked HG complex with a low probability of efficient drug release was stabilized by two supramolecular effects: (i) the close proximity and interaction of the positively charged Pt(II) core and the negative oxygen rim of CB7, and (ii) the strong binding of the adamantyl group of the guest with the CB7 host. The solution for optimized binding can be either putting a molecular linker (spacer) in between the Pt(II) core and the supramolecular anchor (adamantyl) or choosing a weaker anchor with less affinity for the CB7 host or both.

In this account, we proceed with synthesizing **pyPt**-based derivatives **1–4** where the supramolecular anchor is attached at position 4 of the pyridine ring (Fig. 2). First, the pyridine acts as a spacer group between the Pt(II) core and the adamantyl anchor to increase their distance and reduce the attractive electrostatic interaction between the Pt drug (**1** or **2**) and the CB7 carrier in the HG complex. Second, the phenyl and pentafluorophenyl anchors installed at position 4 of pyridine in compounds **3** and **4**, respectively, have a significantly lower affinity for CB7 than the adamantyl group.[40,41] This would result in weaker HG binding and more efficient release of the Pt drug.

In the following, we first investigate the effect of the pyridine-based ligand attached to the platinum core (4-R-pyridine in Fig. 2) on the substitution of chloride by water (aquation)[42] in an HG complex. This chloride aquation is an equilibrium reaction (affected by the concentration of chloride in the solu-

Open Access Article. Published on 23 October 2024. Downloaded on 2/12/2026 1:15:43 AM.
This article is licensed under a Creative Commons Attribution 3.0 Unported Licence.

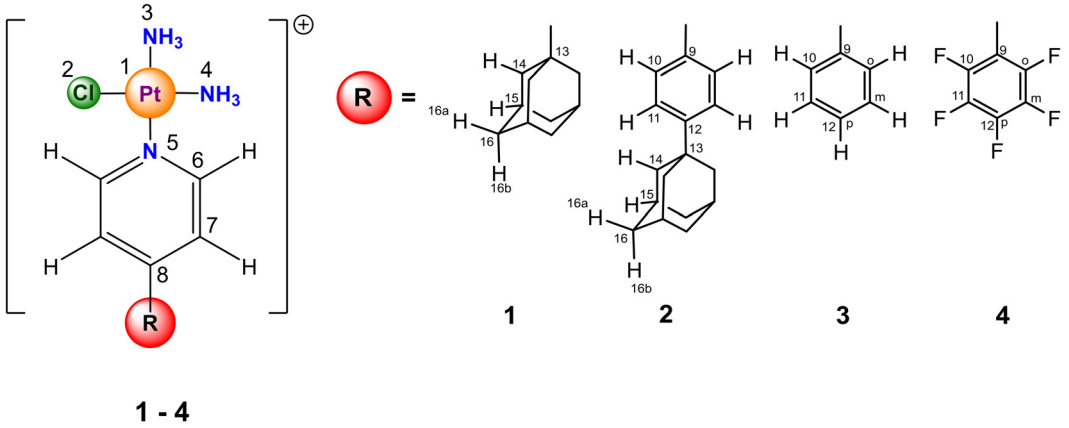

Fig. 2 Structures and atomic numbering scheme for compounds **1–4**.

tion),[39] and is generally considered to be a chemical activation of platinum(II) drugs related to their biological activity.[43] Therefore, in the second step, compounds **1–4** and their HG complexes are tested for cytotoxicity in A2780 cell lines.

Results and discussion

Structure, solubility, and stability of compounds 1–4

Cisplatin was synthesized as described in the review by Lippard[44] and references reported therein. It was used as a starting material for the preparation of compounds **1–4** with the general structure *cis*-$[Pt(NH_3)_2Cl(4\text{-R-py})]^+$ shown in Fig. 2, and as a reference for biological screening. Compounds **1–4** were synthesized by a two-step process similar to that described in our previous work,[39] see the section Materials and methods. The products were extracted as pale white solids and characterized mainly by using mass spectrometry and NMR spectroscopy (see Fig. S1–S27 in ESI†). The molecular structure of compound **3** determined by using single-crystal X-ray diffraction is shown in Fig. 3.

Because of the aim to biologically screen compounds **1–4**, we performed tests of their solubility and stability in an aqueous medium. The solubility was determined from the content of platinum in saturated aqueous solutions of compounds **1–4** and their HG complexes with CB7 (reported value for cisplatin reference ~1–2.5 mg mL^{-1}),[45] using ICP-MS experiments (see Materials and methods). Note that compound **2** was poorly soluble in water due to the presence of the hydrophobic 4-(4′-(1-adamantyl)phenyl)pyridine ligand.

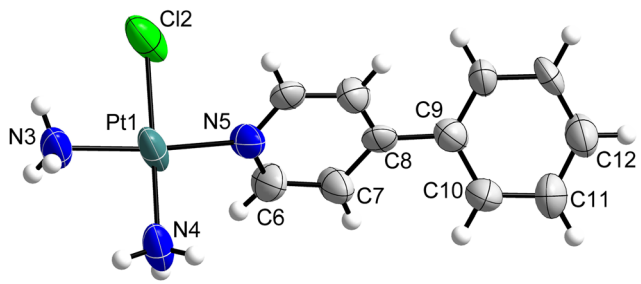

Fig. 3 Molecular structure of compound **3** determined by single-crystal X-ray diffraction (thermal ellipsoids at the 75% probability level; counter anion omitted for clarity). The inter-plane angle between the pyridine and benzene rings is 39° (31° for the DFT-minimized structure).

Adamantyl-based compounds **1** and **2** were less soluble in water than cisplatin (~5.3 mM). The solubility of compound **1** amounts to approximately 2.1 mM, whereas that of **2** is as low as ~1.0 mM. Upon addition of CB7 we identified a notable increase in solubility for both systems (Fig. S27 in ESI†); formation of the HG complex with the CB7 macrocycle results in a more than 4-fold increase in the solubility of **1** (~9.2 mM) and an almost 2-fold increase for **2** (~1.8 mM). Compound **3** (~10.5 mM) was slightly more soluble in water than cisplatin under our conditions, whereas the solubility of compound **4** (~4.9 mM) was comparable to that of cisplatin. However, the effect of the CB7 carrier on the solubility of both compounds **3** and **4** was weakly negative – their solubility decreased slightly in the presence of CB7 (Fig. S28 in ESI†). We hypothesize that this slight decrease in solubility could be due to the formation of less soluble higher associates. However, this assumption will require future in-depth study.

Because of the low solubility of compound **2** in water, we focused our further investigation of stability on compounds **1**, **3**, and **4**. As these compounds dissolved in water, they began to replace the chloride ligand with water in an aquation process ($[PtN_3Cl]^+ \rightarrow [PtN_3(H_2O)]^{2+}$ or $[PtN_3(OH)]^+$; for the ^1H NMR spectra of compound **1**, see Fig. S13 and S14†).

To investigate the effect of HG complexation on the aquation, compounds **1–4** were mixed with CB7 (~1 mM) in aqueous solution. As expected, the adamantyl anchor (156 $Å^3$) of **1** and **2** is strongly bound in the CB7 cavity (242 $Å^3$),[46] whereas the aromatic axles of **3** and **4** are weakly bound because of their smaller size (124 and 136 $Å^3$) and their related less favorable steric fit with the interior of the CB7 barrel (51% and 56%).[46] The process of aquation and the structure–activity

This journal is © the Partner Organisations 2024

Open Access Article. Published on 23 October 2024. Downloaded on 2/12/2026 1:15:43 AM.
This article is licensed under a Creative Commons Attribution 3.0 Unported Licence.

relationship of the HG complexes were studied using a range of NMR techniques and mass spectrometry. The aquation profiles for compounds **1–4** in the presence of CB7 will be thoroughly discussed in the next sections.

Host–guest systems of compounds bearing adamantyl ligand

As indicated above, the CB7 has a high affinity for the adamantyl group (hydrophobic effect in water) as well as cations (electrostatic attraction).[40] To reduce the strong attractive electrostatic interaction of the Pt(II) core in **adaPt** and the CB7 oxygen rim,[39] we inserted a pyridine linker in between the platinum and the adamantyl anchor in compound **1** and an even longer 4-phenylpyridine linker in compound **2**.

The host–guest (HG) complex was prepared by mixing **1**, *cis*-$[Pt(NH_3)_2Cl$(4-(1-adamantyl)pyridine)$]^+$, and **2**, *cis*-$[Pt(NH_3)_2Cl$(4-(4′-(1-adamantyl)phenyl)pyridine)$]^+$, with CB7 (ratio 1 : 1.1) resulting in **1@CB7** and **2@CB7**, respectively. Like **adaPt@CB7** reported previously,[39] in solution both HG systems underwent subsequent transformation at the platinum center, however, to different degrees of aquation. Whereas compound **1** converted to the aqua form **1_aq** at approximately 10% in the absence of the host (see Fig. S13 in ESI†), upon mixing with CB7, the spontaneous aquation of **1** amounted to approximately 35% conversion in one week (Fig. 4 and Fig. S15†). The structure of the transformed HG complex **1_aq@CB7** was confirmed by preparing the aqua form of **1** using $AgNO_3$ (see Materials and methods) and mixing **1_aq** with CB7 (Fig. 4).

These results indicate that incorporating a pyridine spacer in compound **1** significantly attenuates the degree of aquation as compared to that for **adaPt@CB7** where aquation above 90% was observed in one day.[39] It can be predicted that the even longer linker in compound **2** will result in a further attenuation of the aquation in the HG complex **2@CB7**. Indeed, this was observed in the NMR experiments recorded in an identical time window, as shown in Fig. 4 (see also Fig. S18†).

We note that interaction of β-cyclodextrin (β-CD) with compound **1_aq** results in a weak-medium HG binding ($pK_a \sim 5.7$) in a fast exchange regime (averaging of NMR signals at the experimental temperature, Fig. S17a†).

Host–guest systems of compounds bearing an aromatic ligand

To eliminate the effect of the strongly attractive hydrophobic interaction between the adamantyl anchor and the internal cavity of the CB7 barrel, we resorted to compounds **3**, *cis*-[Pt$(NH_3)_2Cl$(4-phenylpyridine)$]^+$, and **4**, *cis*-$[Pt(NH_3)_2Cl$(4-

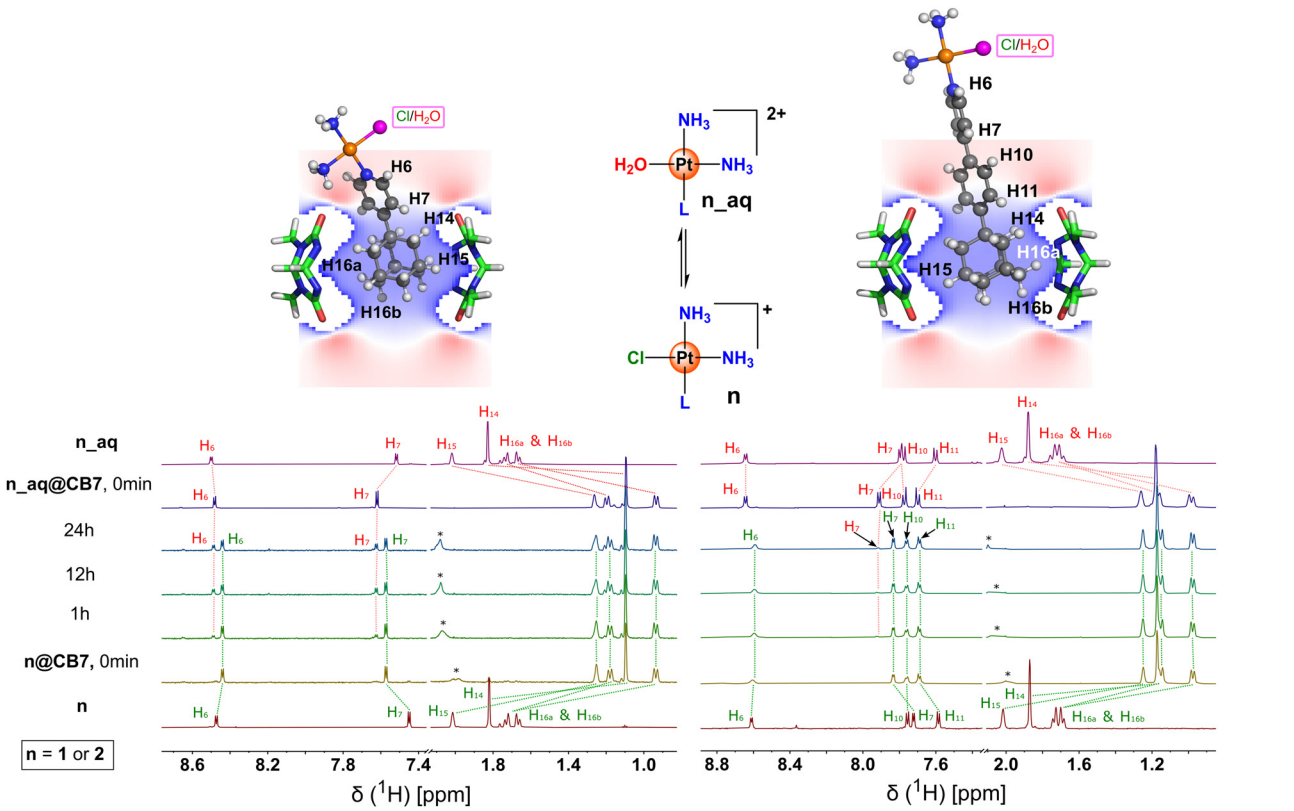

Fig. 4 ^{1}H NMR spectra of **1** (left) and **2** (right), and their aqua forms (**1_aq**, **2_aq**) and HG complexes with CB7. The spontaneous **Pt@CB7** → **Pt_aq@CB7** transformation is indicated in the NMR spectra recorded in a time window of 0–24 hours (for longer times up to 7 days, see ESI†) after the preparation of the **Pt@CB7** sample in D_2O. An impurity in the CB7 sample is labelled with an asterisk (*). A nucleus independent chemical shift (NICS) map of free CB7 (calculated at the RI-B3LYP/def2-TZVPP/VAC level and symmetrized with respect to the axis of rotation of CB7) projected into the molecular model of the inclusion complex **Pt@CB7** (for details, see Materials and methods) is also shown (shielding in blue, deshielding in red).

Open Access Article. Published on 23 October 2024. Downloaded on 2/12/2026 1:15:43 AM.
This article is licensed under a Creative Commons Attribution 3.0 Unported Licence.

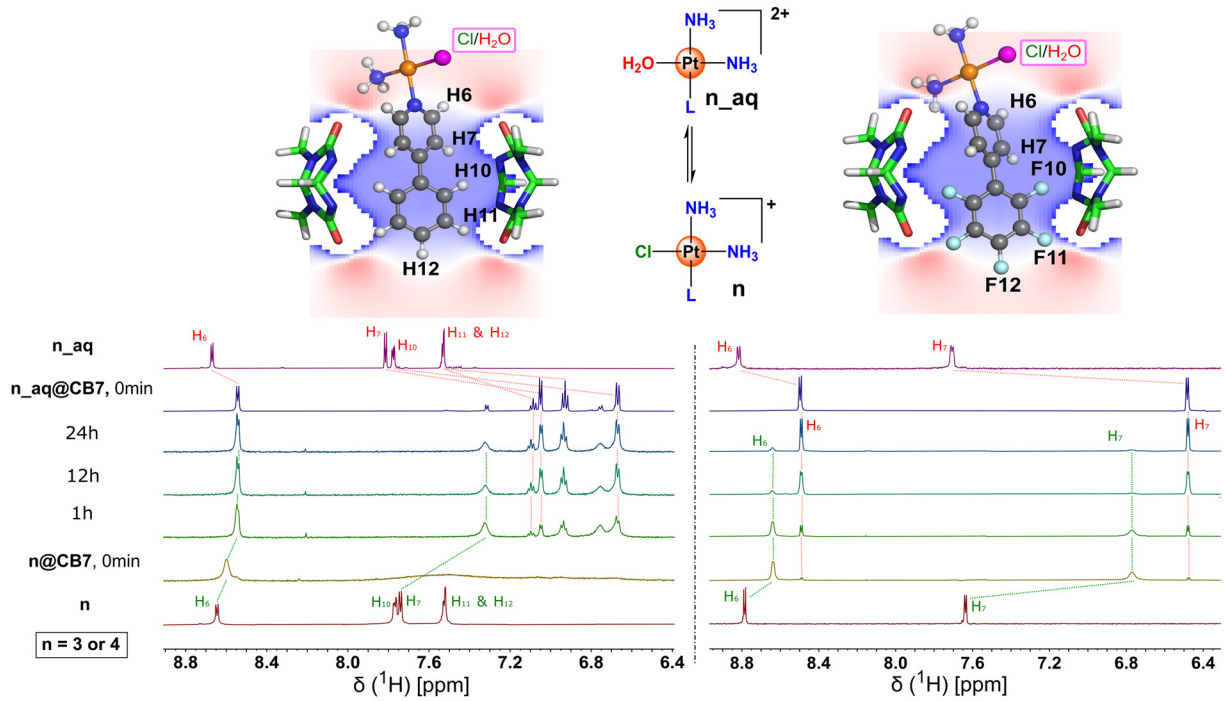

Fig. 5 ^{1}H NMR spectra of **3** (left) and **4** (right), their aqua forms (**3_aq**, **4_aq**), and HG complexes with CB7. The spontaneous **Pt@CB7** → **Pt_aq@CB7** transformation is indicated in the NMR spectra recorded in the time window of 0–24 hours after the preparation of the **Pt@CB7** sample in D_2O. A nucleus independent chemical shift (NICS) map of free CB7 (calculated at the RI-B3LYP/def2-TZVPP/VAC level) projected into the molecular model of the inclusion complex **Pt@CB7** (for details, see Materials and methods) is also shown (shielding in blue, deshielding in red).

pentafluorophenylpyridine)]$^+$, Fig. 2. The interaction of **3** and **4** with CB7 resulting in **3@CB7** and **4@CB7**, respectively, is accompanied by a significant broadening of the ^{1}H NMR resonances in the aromatic region (Fig. 5).

This broadening indicates that a dynamic process occurs for the non-aquated HG complex **Pt@CB7**. Generally, the NMR line broadening for these systems can originate either in an exchange process between the free and bound forms (**Pt** ↔ **Pt@CB7**) or the internal supramolecular conformational dynamics of sliding the CB7 wheel along the 4-phenylpyridine axle in **Pt@CB7** or both. The concentration-dependent line broadening of ^{1}H NMR lines (Fig. S3†) indicates that some role is played by the free ↔ bound equilibrium. Note the somewhat less pronounced line broadening for **4@CB7** in Fig. 5, indicating slower free ↔ bound exchange and a better-defined position of the guest in the HG complex (for calculated binding profiles, see ESI†). However, the internal supramolecular conformational dynamics allow the platinum core of the guest to come into close contact with the oxygen portal of the CB7 host, and their electrostatic stabilization promotes shifting the equilibrium towards the encapsulated aqua form. In other words, the aqua form (**Pt_aq@CB7**) is more strongly bound in the HG complex, and its dynamics is suppressed. This aquation accompanied by the increased rigidity of the HG complex is clearly revealed in the ^{1}H NMR spectrum in Fig. 5, where a new set of narrow signals belonging to **Pt_aq@CB7** gradually appears in time. In contrast to the **Pt@CB7** complex, the well-resolved ^{1}H NMR resonances of **Pt_aq@CB7** can be assigned to individual atoms using 2D NMR experiments (see Fig. S21 and S22†). (Note that **3_aq** is only weakly bound to β-CD (pK_a = 3.5, Fig. S23†) and the interaction of **4_aq** with β-CD was even undetectable by the standard ^{1}H NMR titration experiment.)

To support our conclusions about the structure and dynamics of **Pt@CB7** and **Pt_aq@CB7** systems, we performed unbiased molecular dynamics (MD) simulations of the four HG complexes and evaluated the average distances between the center of mass of the non-hydrogen atoms of the aromatic ligand of the guest and the plane of symmetry of the CB7 host as shown in Fig. 6.

Effect of aquation. The MD simulation of **3@CB7** points to the relatively shallow average encapsulation of compound **3** in the cavity of CB7 (r_{av} = 1.57 Å) and its barrierless sliding over the broad range of distances indicated by the histogram of distances in Fig. 6a. Upon aquation, compound **3_aq** penetrates more deeply into the CB7 cavity (r_{av} = 1.06 Å) described by three distinct positional minima (see histogram in Fig. 6b). The additional aquation-induced penetration (**3** *vs.* **3_aq**) amounts to ~0.5 Å and results in a more rigid HG complex.

Similar to compound **3**, compound **4** exhibits barrierless sliding in the cavity of CB7 over a broad range of ODIS values (Fig. 6c), whereas three minima were obtained by MD simulation of **4_aq** as shown in Fig. 6d. The difference of ~0.6 Å in the degree of penetration induced by aquation is slightly larger than that for **3** discussed above.

To further support our theoretical findings on the greater degrees of HG penetration upon aquation, we analyzed com-

 This journal is © the Partner Organisations 2024

Open Access Article. Published on 23 October 2024. Downloaded on 2/12/2026 1:15:43 AM.
This article is licensed under a Creative Commons Attribution 3.0 Unported Licence.

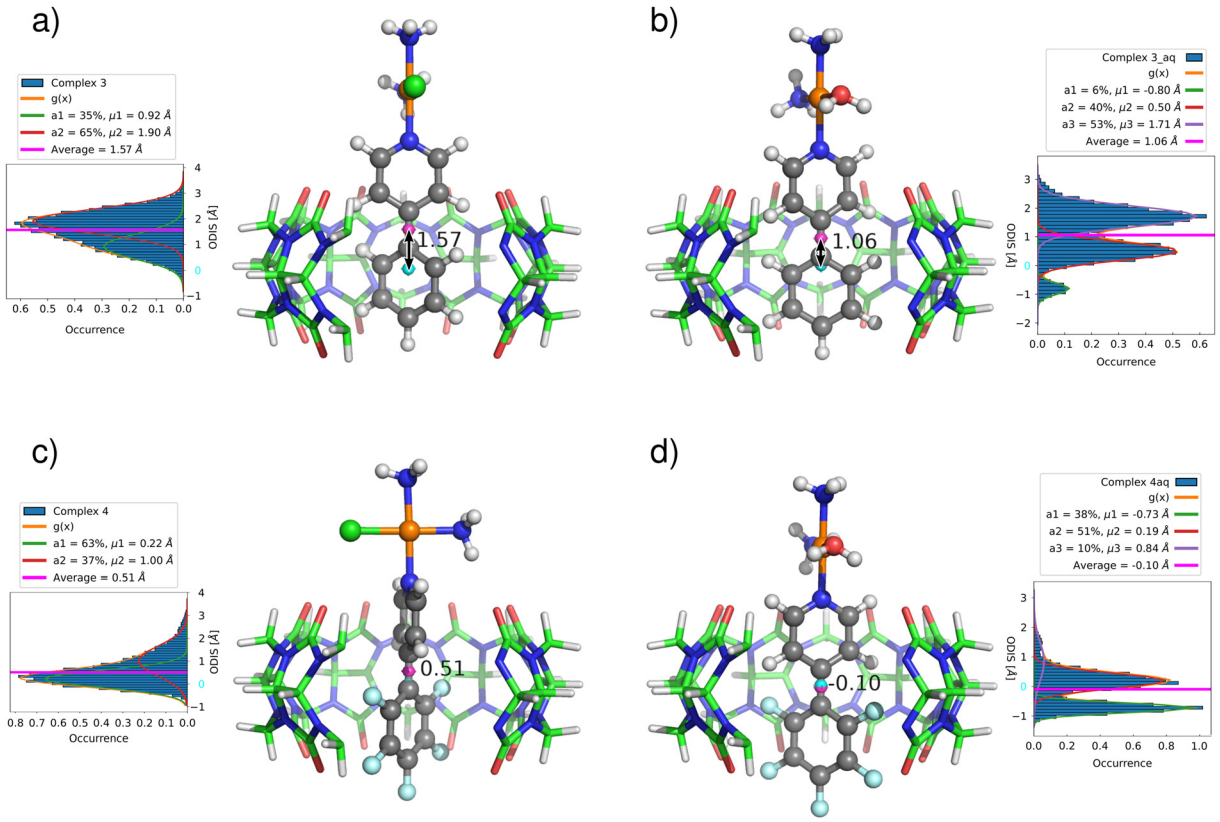

Fig. 6 Average values of intermolecular oriented distances (ODIS in Å) as obtained from unbiased MD simulations of (a) **3@CB7**, (b) **3_aq@CB7**, (c) **4@CB7**, and (d) **4_aq@CB7** with the distribution shown in the form of histograms. The distribution of distances is in good qualitative agreement with the ABF calculation of the free energy profiles. (See Fig. S31 and S32 in ESI.†)

plexation-induced NMR shifts for **3@CB7** and **3_aq@CB7**, as shown in Fig. 7. Indeed, the shielding patterns identified for **3@CB7** (the most shielded region around H10 and H11) and **3_aq@CB7** (the most shielded H10 and H7) correspond to deeper penetration of **3_aq**. The phenomenon of greater shielding of H7 in the aqua form has also been identified for compound **4**.

We also calculated and visualized NMR shielding maps for the CB7 host and calculated the values of the nucleus-independent chemical shifts (NICS) at the positions of the individual hydrogen atoms in all four HG complexes. These data are summarized in Table S5 and discussed thoroughly in ESI.†

Effect of ligand. Comparing the MD simulations of **3** bearing the 4-phenylpyridine ligand (r_{av} = 1.57 Å in Fig. 6a) with those of **4** containing the pentafluorophenyl ring (r_{av} = 0.51 Å in Fig. 6c) indicates a notably deeper encapsulation of **4**. This is supported by analyzing the differences in the NMR shifts of H7 (see Fig. 7). The experimental complexation ^{1}H NMR shifts ($\Delta\delta$) for non-aquated systems revealed that the H7 atom is more shielded for encapsulated **4** than for **3** ($\Delta\Delta\delta$ = −0.4 ppm; the DFT calculations predict the same trend but overestimate the value: $\Delta\Delta\delta$ = −0.7 ppm). A similar difference in the complexation NMR shift ($\Delta\Delta\delta$ = −0.5 ppm) was observed for aquated systems (DFT calculated $\Delta\Delta\delta$ amounts −0.3 ppm). Although the influence of changing the ligand on the H6 resonance is substantially weaker because of its external position, we also observed a weak secondary NMR shielding.

In both cases (**4** and **4_aq**), the ligand-induced degree of penetration exceeds 1 Å and results in a partial protruding of the pentafluorophenyl ring through the opposite CB7 portal. This change in geometry must influence the effectivity of the aquation process (degree of aquation) as already indicated in Fig. 5 and further supported by the ^{19}F NMR spectra shown in Fig. 8.

To support the hypothesis of a deeper penetration by 4-pentafluorophenylpyridine and to determine its position inside the cavity of CB7, we performed ^{1}H–^{1}H ROESY experiments for **3_aq@CB7** and **4_aq@CB7** and measured a 2D heteronuclear ^{1}H–^{19}F NOE experiment (HOESY) for **4_aq@CB7**, see Fig. 9. Indeed, the ^{1}H–^{19}F dipolar contacts (through-space interaction) obtained between F10/F11 of **4_aq** and Ha′ of CB7, the weaker F10-Hc, and the absence of interaction between F12 and the CB7 host confirm the preference for a protruding conformation with a large distance between F12 and CB7.

Ligand effect on the aquation of chloride in HG complexes

The degree of aquation at the Pt(II) center can be easily determined by analyzing the population of the aqua form (**Pt_aq**) from the integrals of the individual ^{1}H NMR signals. We deter-

Open Access Article. Published on 23 October 2024. Downloaded on 2/12/2026 1:15:43 AM.
This article is licensed under a Creative Commons Attribution 3.0 Unported Licence.

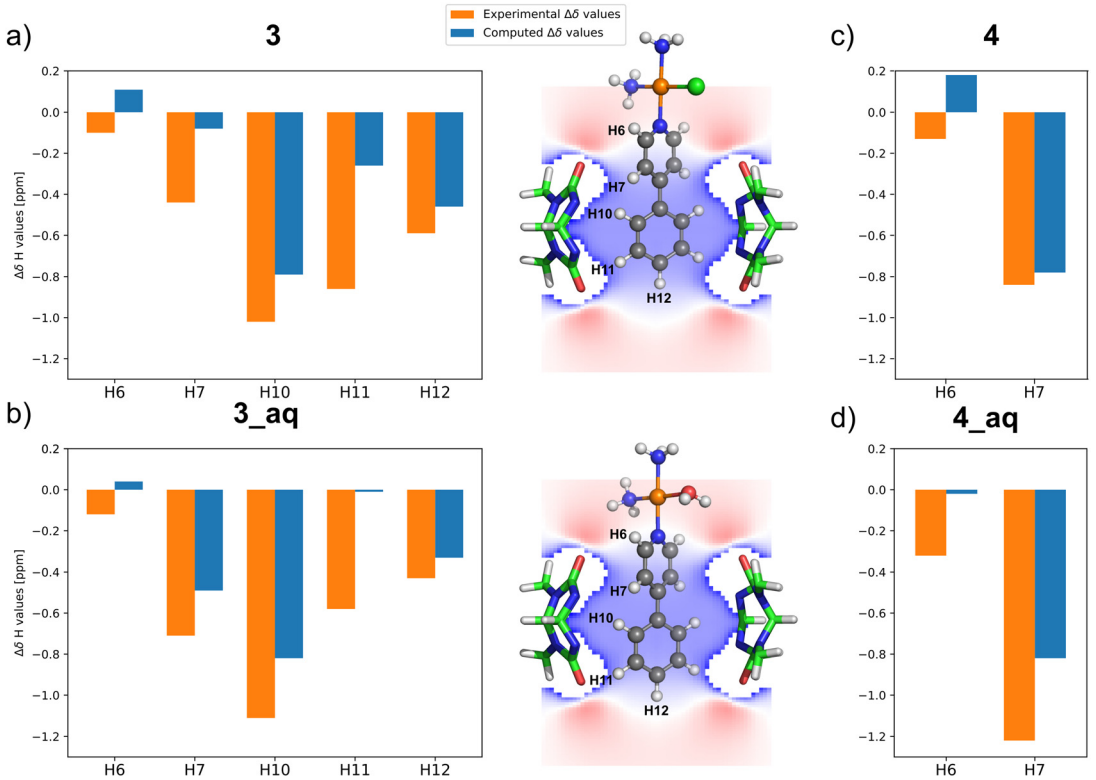

Fig. 7 Complexation-induced (secondary) NMR shifts for compounds (a) **3**, (b) **3_aq**, (c) **4**, and (d) **4_aq** observed experimentally (orange) and calculated (blue) using an explicit model of the inclusion complex (RI-B3LYP/def2-TZVPP/CPCM). The contributions of the individual geometries (for NMR scans, see Fig. S33–S36†) were weighted based on free energy profiles obtained from ABF simulations. For computational details, see Materials and methods.

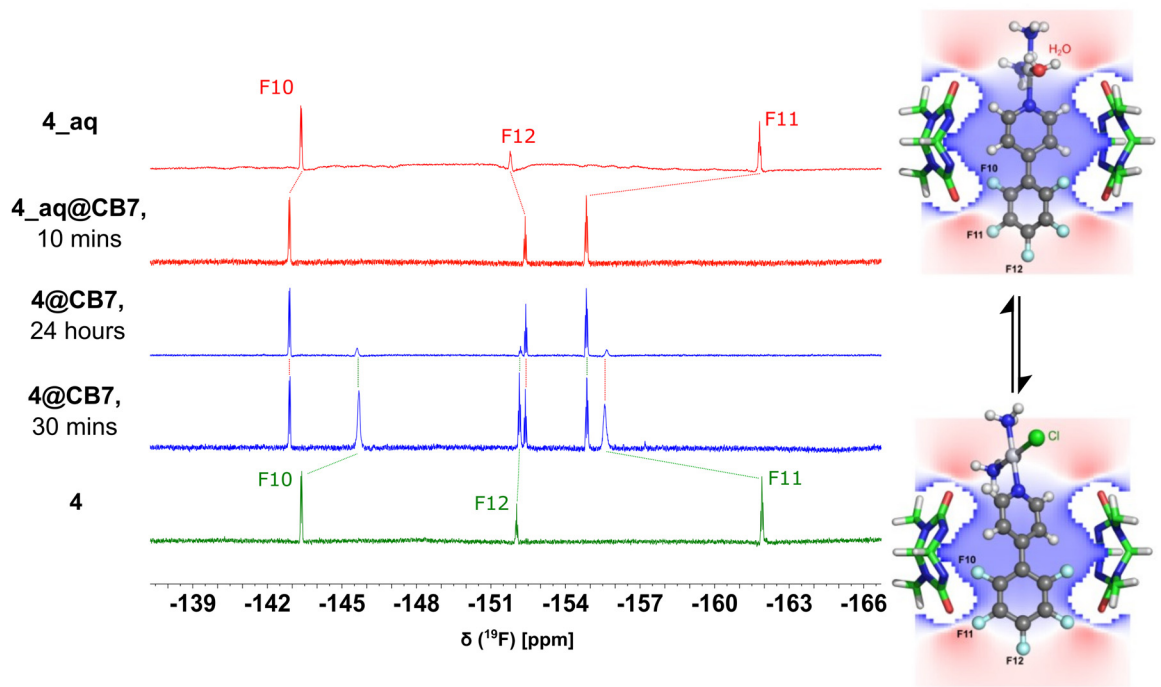

Fig. 8 ^{19}F NMR spectra for compounds **4**, **4_aq**, and their HG complexes with CB7. Note the line broadening for **4@CB7** ascribed to both free-bound and positional encapsulation dynamics.

This journal is © the Partner Organisations 2024

Open Access Article. Published on 23 October 2024. Downloaded on 2/12/2026 1:15:43 AM.
This article is licensed under a Creative Commons Attribution 3.0 Unported Licence.

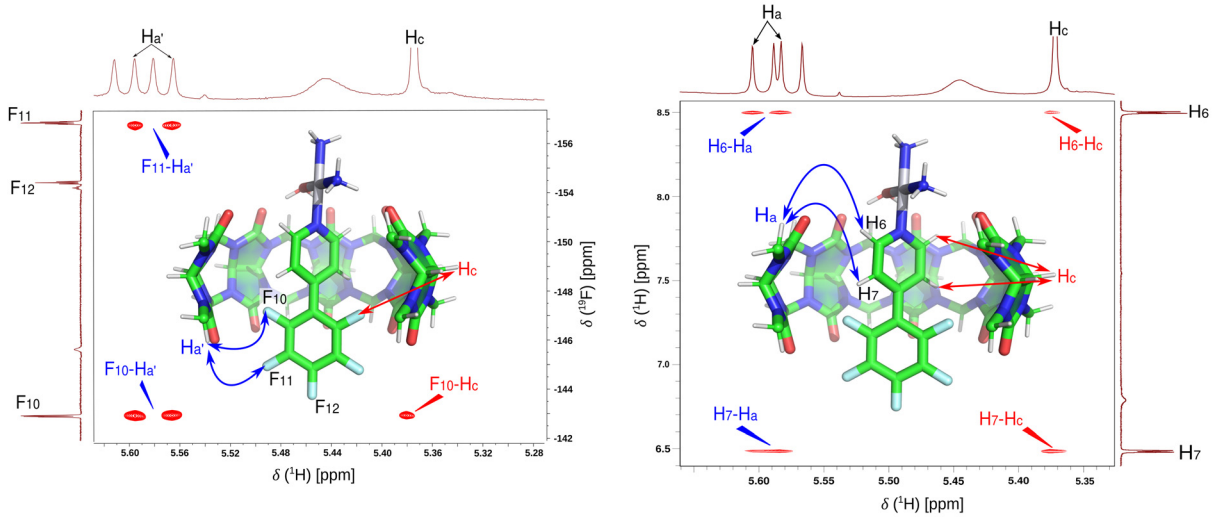

Fig. 9 $^{1}H–^{19}F$ HOESY (left) and $^{1}H–^{1}H$ ROESY (right) spectra of **4_aq@CB7** in aqueous solution (*cf.* $^{1}H–^{1}H$ ROESY of **3_aq@CB7**, Fig. S22 in ESI†).

mined the ratio between the native non-aquated system and the aqua form (non-aquated:aquated; **Pt@CB7:Pt_aq@CB7**) with the sum normalized to 100 (%). As discussed in the previous sections, installing a molecular linker to alter the distance between the platinum center and the oxygen portal of the CB7 results in a significant change in the degree of aquation.

The aquation is almost quantitative (and very fast) for the system **adaPt@CB7** reported previously (Fig. 10a).[39] The 1 : 1 ratio is reached approximately one hour after mixing **adaPt**

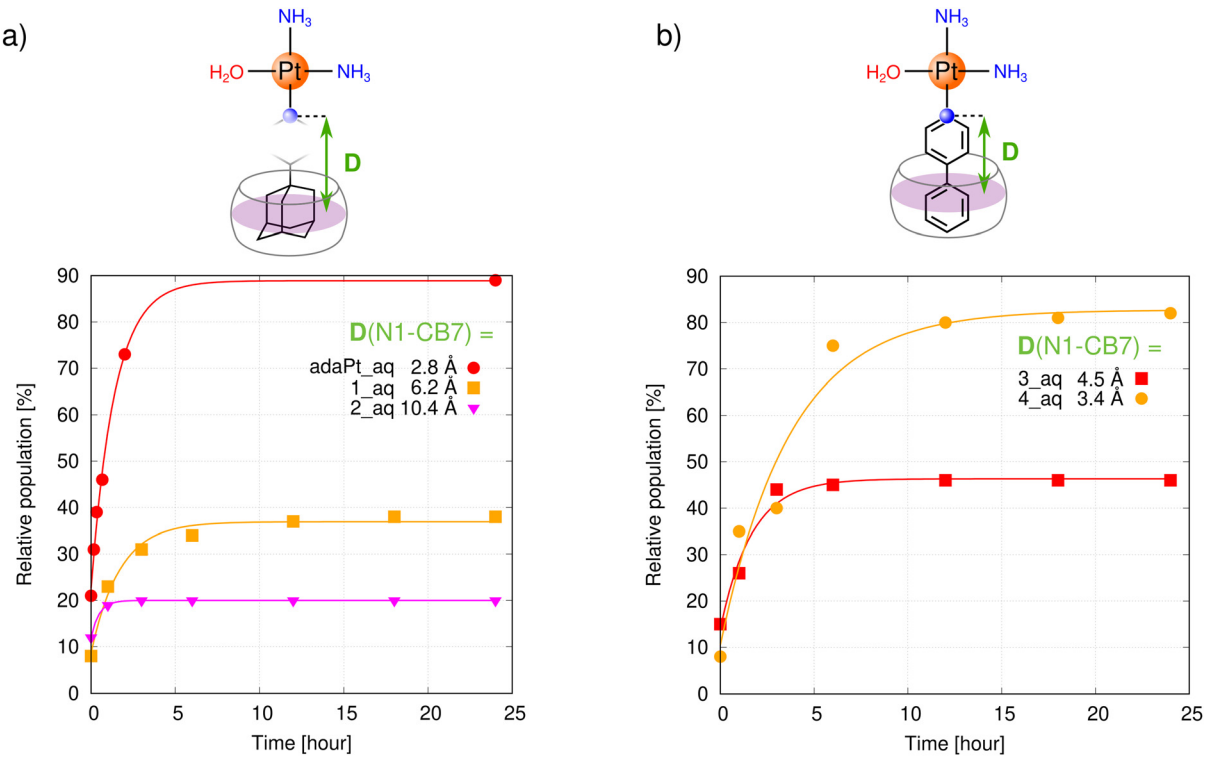

Fig. 10 The aquation process for compounds (a) **adaPt**, **1**, **2** and (b) **3**, **4** in the presence of CB7 (all as 1 mM solutions in a 1 : 1 HG ratio) obtained as the relative population of the aqua form by using ^{1}H NMR spectroscopy. The distance *D* (in Å) corresponds to the average oriented distance of the N1 of pyridine with respect to the central plane of CB7 resulting from unbiased MD simulations (see Materials and methods). (Note that the equilibrium **Pt@CB7** ↔ **Pt_aq@CB7** is influenced by: (i) the stabilities of the bound HG complexes, which govern the populations of the individual forms, (ii) the conformational flexibility of each HG complex, which governs the distribution of distance *D*.)

Open Access Article. Published on 23 October 2024. Downloaded on 2/12/2026 1:15:43 AM.
This article is licensed under a Creative Commons Attribution 3.0 Unported Licence.

with the CB7 host, and the guest is almost completely converted to **adaPt_aq@CB7** (10 : 90) in 24 hours. The pyridine linker between the adamantyl anchor and the platinum center in **1** reduces the degree of aquation substantially compared to **adaPt**; a near-equilibrium ratio of 65 : 35 is reached in about 24 hours (Fig. 10a). The even longer 4-phenylpyridine linker in **2**, separating the adamantyl anchor and the platinum to the electrostatically almost ineffective distance of 10.4 Å, restricts conversion to the aqua form **2_aq@CB7** to only about 20% in 24 h (80 : 20; Fig. 10a).

The axles 4-phenylpyridine and 4-pentaflurophenylpyridine in **3** and **4**, respectively, have very similar volumes but significantly different distributions of electron density due to the different electronegativities of the five surface atoms at the terminal part of the axle (H *vs.* F on phenyl). The average distance (*D* in Fig. 6) between the nitrogen N1 and the centroid of the atoms of the CB7 in **3_aq@CB7** is approximately 4.5 Å, which is similar to that in **1_aq@CB7** (6.2 Å). Thus the ratio 55 : 45 for **3@CB7** in 24 h (Fig. 10b) roughly resembles that for **1@CB7** discussed above (65 : 35). In contrast, deeper penetration of the 4-pentaflurophenylpyridine axle in **4@CB7** makes the "electrostatic" distance between N1 and CB7 shorter (the average *D* is 3.4 Å, Fig. 10b) and the conversion of **4@CB7** to **4_aq@CB7** is more efficient (20 : 80 after 24 h, Fig. 10b). In summary, different supramolecular interactions (weak hydrogen bonding for **3** *vs.* O···F and H···F electrostatics for **4**) between the phenyl or pentafluorophenyl ring and the CB7 portal induces different degrees of penetration and aquation.

The degree (and time-dependence) of chemical activation by aquation of the platinum compounds by the CB7 carrier should be reflected in the (time-dependent) cytotoxicity of compounds **1–4** and their uptake by cells. This assumption is investigated and discussed in the next section.

Biological screening: time-dependent cytotoxicity and uptake

The cytotoxicity of compounds **1**, **3**, **4** (compound **2** is insufficiently soluble in the medium) and their supramolecular complexes with β-CD and CB7 was tested using two cell lines: A2780 (an ovarian cancer cell line) and A2780/CP (a cisplatin-resistant ovarian cancer cell line). The IC_{50} values were determined after 24 and 48 hours and were compared to those for cisplatin, the reference used. Note that the cytotoxicity of the reference cisplatin is only marginally affected by its 1 : 1 mixing with β-CD or CB7 because cisPt forms relatively weak HG complexes with CB7 [32] and β-CD.[47]

Our previously reported compound **adaPt**, *cis*-[$Pt(NH_3)_2Cl$(1-adamantylamine)]NO_3, showed moderate toxicity against the A2780 (80 μM after 48 h) and A2780/CP (110 μM, 48 h) cell lines.[39] The formation of an HG complex with CB7 reduced the cytotoxicity significantly despite the very fast drug activation by aquation substitution of the chloride ligand. This discovered supramolecular bio-protection by CB7 (2–3 times larger IC_{50})[39] derived from the formation of the strong HG complex **adaPt_aq@CB7**.

The degree of aquation can be modulated by

(i) changing the distance between the platinum center and the oxygen portal of CB7, and

(ii) the HG binding constant, which can be tuned by changing the nature of the supramolecular anchor. Both factors have been explored in this study.

First, we introduced a longer linker between the platinum center and the adamantyl anchor in compound **1** (pyridine *vs.* $-NH_2$) aiming to reduce the rate of aquation (*cf.* Fig. 10). Unfortunately, the cytotoxicity of compound **2** with an even longer linker was not determined because of its poor solubility in the culture medium (and water). The cytotoxicity of compound **1** against A2780 (38 μM after 48 h) and A2780/CP (75 μM, 48 h) cell lines was somewhat greater than that for **adaPt**, Fig. 11. This could result from the presence of the planar pyridine ring that is attached to platinum and assists in binding compound **1** to base pairs in DNA.[24] Importantly, the effectivity of the biological protection of this compound afforded by CB7 (3–4 times larger IC_{50}) is very similar to that for **adaPt**.

Second, we developed compounds **3** and **4** with phenylpyridine axles lacking a strong supramolecular anchor. These compounds were designed to reduce affinity for CB7 ($pK_a \sim 5$ for compound **4_aq**, see Fig. S23b in ESI†),[48] and to show more effective release compared to **adaPt** and **1** ($pK_a \sim 7.5$ for compound **1_aq**, see Fig. S17b in ESI†). However, their binding with the investigated macrocycles is probably too weak, which results in a negligible change in IC_{50} values upon the formation of HG complexes (Fig. 11).

Unexpectedly, the cytotoxicity of compound **3** against A2780/CP after 48 h was comparable to that of cisPt and significantly exceeded that of the archetype pyriplatin against this cisplatin-sensitive cell line.[49] This could indicate slower accumulation of the drug in the cell but also an inefficient release that could possibly lead to overcoming an intrinsic or acquired resistance. The observed properties open the door for the further structure–activity tuning of compound **3**. To tailor it further, we designed compound **4** bearing five fluorine atoms on the aromatic ring. Its cytotoxicity is comparable to that of cisPt for the sensitive A2780 cell line at 24 h (Fig. 11) but, unfortunately, drops for longer exposure and for the A2780/CP line.

To gain additional insight into modulation of the cytotoxicity attributable to the introduced structural changes and the formation of HG complexes as delivery vehicles for the Pt (II) cargo, we determined the uptake of platinum by A2780 and A2780/CP cells in 24 and 48 hours. The experiments were performed uniformly using a concentration of 2.5 μM (sub-IC_{50} for cisplatin) for all compounds and their supramolecular complexes. The treated cell samples were analyzed by using ICP-MS to determine their content of Pt (given in ng per 10^9 cells in Fig. 12).

Compounds **1** and **3** were initially (24 h) better received by A2780 than cisplatin, probably because of the presence of the lipophilic pyridine linker with an adamantyl anchor (**1**) or the aromatic phenylpyridine axle (**3**). As expected, CB7 reduced the uptake for **1** but slightly increased the accumulation for cisPt as reported previously.[50] The less efficient uptake of CB7-protected compound **1** correlates nicely with the lower cytotoxicity of this HG complex (larger IC_{50} values).

 This journal is © the Partner Organisations 2024

Open Access Article. Published on 23 October 2024. Downloaded on 2/12/2026 1:15:43 AM.
This article is licensed under a Creative Commons Attribution 3.0 Unported Licence.

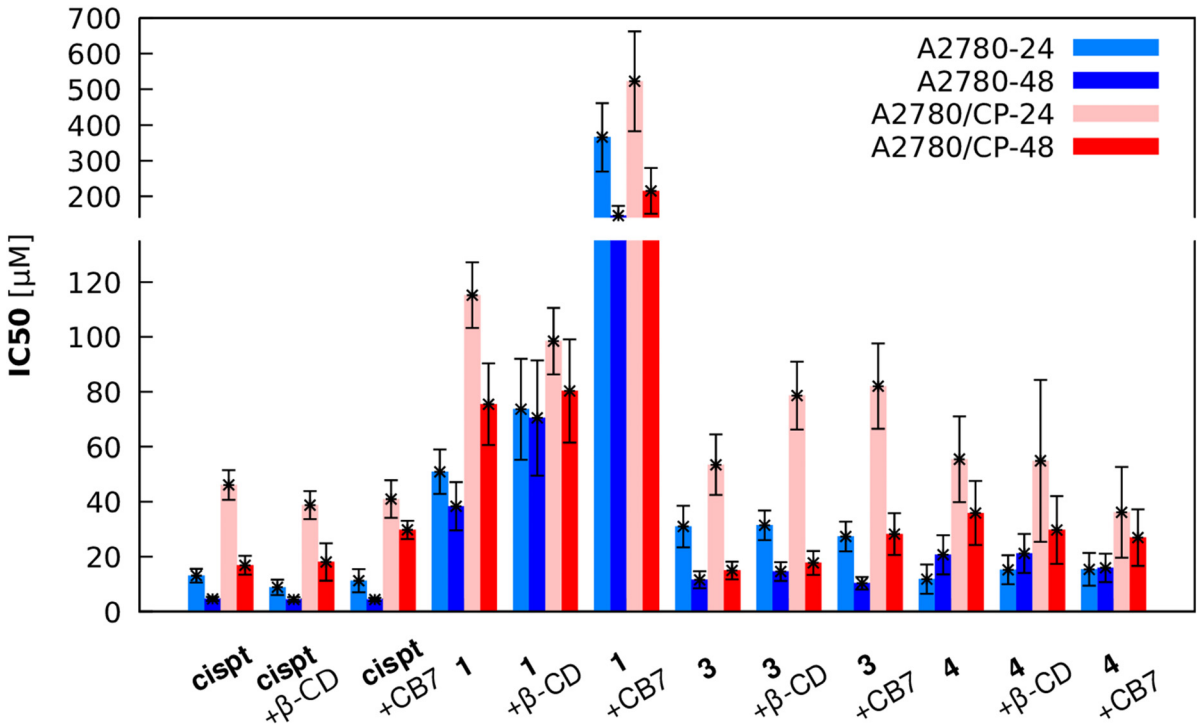

Fig. 11 IC_{50} values for reference **cisPt** and compounds **1**, **3**, and **4** and their HG complexes with β-CD and CB7. The values are shown for the cisplatin-sensitive A2780 (blue) and cisplatin-resistant A2780/CP (red) cell lines, determined after 24 (light) and 48 (dark) hours.

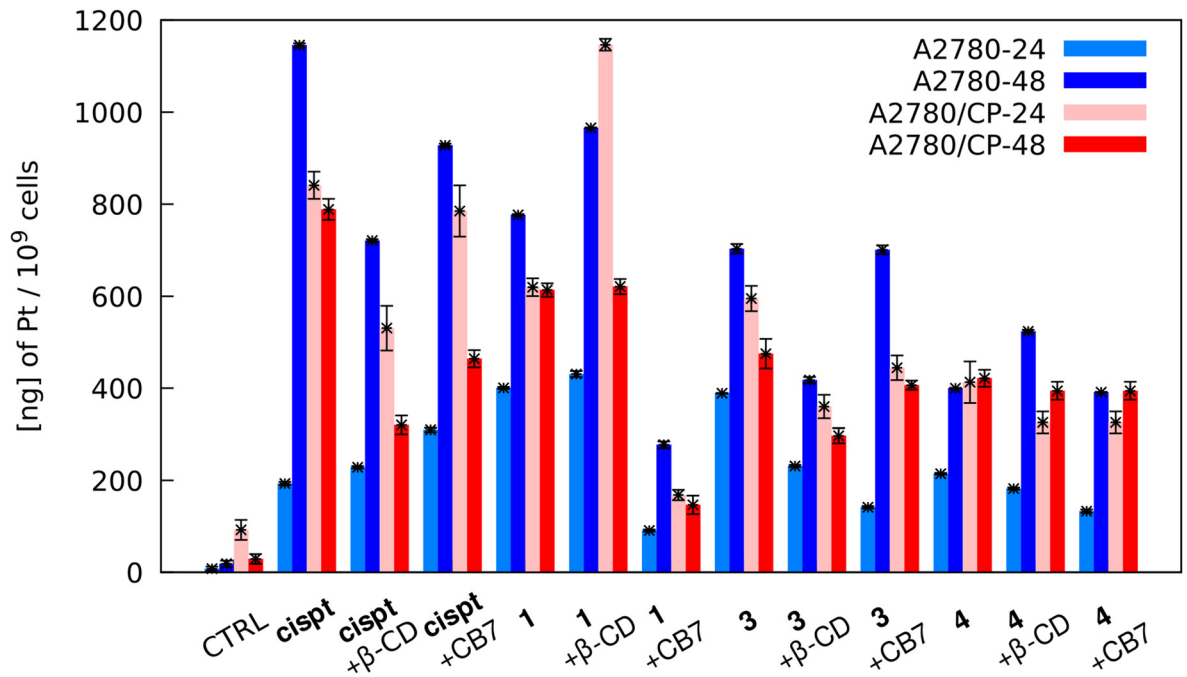

Fig. 12 Cellular uptake of **cisPt**, compounds **1**, **3**, and **4**, and their HG complexes. Cisplatin-sensitive A2780 (blue) and cisplatin-resistant A2780/CP (red) cell lines observed after 24 (light) and 48 (dark) hours.

Note that, as expected, the platinum uptake for the A2780 cell line increases with time in all cases, but the cisplatin-resistant cell line A2780/CP is prone to excrete the drug (platinum) by developed cellular mechanisms over time. Thus, A2780/CP has much faster drug uptake than A2780 (2–5 times larger values after 24 h), but also an

Open Access Article. Published on 23 October 2024. Downloaded on 2/12/2026 1:15:43 AM.
This article is licensed under a Creative Commons Attribution 3.0 Unported Licence.

efficient drug-releasing mechanism (comparable or smaller numbers after 48 h).

As discussed in our previous paper,[39] β-CD notably enhanced the accumulation of the adamantyl-based system **adaPt** in cells, which can also be seen for compound **1** in Fig. 12. However, this higher accumulation has a vanishingly small effect on the cytotoxicity. Therefore, this accumulation could originate in the cyclodextrin-mediated association of compound **1** with the cellular wall. Our hypothesis deserves to be investigated thoroughly in the future.

In summary, highlighting the observations for both of the cell lines investigated (A2780, A2780/CP) and the exposure times (24 and 48 h), the conversion of cisPt to compound **1** by installing a 4-(1-adamantyl)pyridine ligand instead of chloride results in 4–5 times lower cytotoxicity. In addition, trapping the adamantyl anchor of compound **1** in CB7 reduces the cytotoxicity by a further 3–7 times. This behavior offers great potential for protected platinum delivery if an additional structural modification could, on demand, allow the recovery of **cisPt** or its selective modification. Further research in this direction is underway in our laboratory.

Conclusions

In this work, we successfully synthesized derivatives of pyriplatin containing an adamantyl anchor or an aromatic axle that was used for binding with a cucurbit[7]uril macrocycle (CB7) to influence the aquation of a chloride ligand at a Pt(II) core.

The degree of aquation in the presence of CB7 depends on the structure of the inclusion host–guest complex, namely, the effective distance between the platinum center of the guest and the oxygen portal of the host. Thus, for adamantyl-based systems (**1** and **2**) the degrees of aquation are low because the CB7 host is strongly bound to the distant adamantyl anchor and does not significantly influence the Pt(II) core. In contrast, the weaker HG binding of the aromatic phenylpyridine axles in **3** and **4** allow for a shorter distance between the chloride ligand on platinum and the oxygen portal of CB7, thereby enhancing the degree of aquation. The difference between compounds **3** and **4** is shown to originate in the different degrees of penetration into the CB7 host induced by different supramolecular interactions which involve weak attractive hydrogen bonding for **3** and repulsive O···F and attractive H···F electrostatic interactions for **4**. The latter results in a partial expulsion of the pentafluorophenyl unit from the second CB7 portal, but brings the platinum core closer to the first CB7 portal inducing efficient aquation.

The time-dependent toxicity of compounds **1**, **3**, and **4** and their HG complexes was determined against ovarian cancer cell lines A2780 and A2780/CP after 24- and 48-hours of exposure. All the compounds were more cytotoxic than the parent pyriplatin (comparing to reported values for **pyPt**)[49] but less toxic than cisplatin, the reference used. As expected, drug (platinum) accumulation increased with time for the A2780 cell line, whereas the opposite trend was obtained for the cisplatin-resistant A2780/CP cell line because releasing mechanisms developed.[51] In general, notable uptake was observed for compounds **1** and **3** (comparable to **cisPt**) but their cytotoxicity was lower than that of **cisPt**.

The HG complex **1@β-CD** is also little cytotoxic despite its effective association with the cells. Analogous behavior had been observed previously for **adaPt** combined with β-CD.[39] We hypothesize that this can be linked not to the cell penetration of the drug but rather the association of the drug with the cell wall mediated by β-CD. This behavior deserves further study.

In general, the assembly of synthesized compounds with β-CD modulates the cytotoxicity negligibly, probably because of weak HG binding and the predominance of free forms of the drugs in the solution. Similarly, the formation of weak HG complexes of compounds **3** and **4** with CB7 does not modulate their cytotoxicity. In contrast, the strong HG complex of **1** with CB7 increases IC_{50} values significantly. The prospective combination of the behavior of compounds **1** and **3** in molecular design will open a new direction in supramolecular platinum-drug activity and delivery.

Materials and methods

Analytical methods

Mass spectrometry. Electrospray ionization mass spectrometry (ESI-MS) measurements were acquired on an Agilent 6224 Accurate-Mass TOF LC-MS.

NMR spectroscopy. ^{1}H, ^{13}C, and ^{195}Pt NMR spectra were recorded on a Bruker Avance III HD 700 MHz spectrometer (BBO or BBI probe) at 298 K, if not stated otherwise. ^{1}H and ^{13}C NMR spectra were referenced internally to the signal of the solvent,[52] DMSO-d_6 [^{1}H (δ = 2.5 ppm) and ^{13}C (δ = 39.52 ppm)], $CDCl_3$ [^{1}H (δ = 7.26 ppm) and ^{13}C (δ = 77.16 ppm)], and NMR chemical shifts were reported relative to tetramethylsilane, TMS (δ = 0 ppm). ^{195}Pt NMR spectra were recorded in D_2O for locking purposes, referenced to K_2PtCl_6. ^{19}F NMR was measured in D_2O using trifluoroacetic acid as reference (δ = −76 ppm).

X-ray diffraction. Monocrystals of compound **3** suitable for X-ray diffraction were grown by slowly diffusing diethyl ether into a DMF solution containing compound **3**. Diffraction data were collected on a Rigaku MicroMax-007 HF rotating anode four-circle CCD diffractometer with Mo Kα radiation. The temperature during data collection was 120(2) K. The structures were solved by direct methods and refined by full matrix least-squares methods using SHELXT[53] and SHELXL.[54] Crystallographic data and structural refinement parameters are available from CSD, CCDC no. 2371255.†

Chemical syntheses

Chemicals. Potassium tetrachloroplatinate, cucurbit[7]uril, β-cyclodextrin, and other chemicals, and solvents were purchased from Sigma-Aldrich Co., Alfa Aesar, and abcr GmbH. The *cis*-$PtCl_2(NH_3)_2$ and *trans*-$PtCl_2(NH_3)_2$ were synthesized as described in the review by Lippard[44] and references reported

 This journal is © the Partner Organisations 2024

Open Access Article. Published on 23 October 2024. Downloaded on 2/12/2026 1:15:43 AM. This article is licensed under a Creative Commons Attribution 3.0 Unported Licence.

therein. Pyridine-based ligands 4-(1-adamantyl)pyridine, 4-(4′-(1-adamantyl)phenyl)pyridine, and 4-pentafluorophenylpyridine were prepared as described in ESI.†

*Synthesis of **1**.* To a solution of cisplatin (0.16 mmol, 50 mg) in 10 mL DMF, $AgNO_3$ (0.16 mmol, 27 mg) was added. The reaction mixture was stirred in the dark at 60 °C for 24 hours. Then, the AgCl precipitate was filtered off and to the supernatant 0.9 equivalent of 4-(1-adamantyl)pyridine (0.14 mmol, 30 mg) was added and the reaction mixture was stirred for 24 hours at 60 °C. To the clear reaction mixture, 10 mL of methanol was added. Then, 30 mL of diethyl ether was added to precipitate the product. The white product precipitate was filtered out and washed with 10 mL of diethyl ether. This procedure was repeated 3–5 times to remove all the residual DMF from the mixture and obtain the pure product.

1. Yield: 48%. ^{1}H NMR (700 MHz, DMSO-d_6): δ = 1.74 (d, 6H, CH_2), 1.87 (s, 6H, CH_2), 2.09 (s, 3H, CH), 4.25 (bs, 3H, NH_3), 4.61 (bs, 3H, NH_3), 7.56 (dd, 2H, CH), 8.60 (dd, 2H, CH) ppm. ^{13}C NMR (700 MHz, DMSO-d_6): δ = 150 (C6), 120.79 (C7), 130.5 (C8), 40.44 (C14), 42.08 (C13), 28.05 (C15), 36.42 (C16) ppm. ^{195}Pt NMR (700 MHz, D_2O): δ = −2298 ppm. ESI-MS(+) *m*/*z* 478.1372 $[C_{15}H_{25}ClN_3Pt]^+$, calc. 478.1370.

*Synthesis of **2**.* To a solution of cisplatin (0.16 mmol, 50 mg) in 10 mL DMF, $AgNO_3$ (0.16 mmol, 27 mg) was added. The reaction mixture was stirred in the dark at 60 °C for 24 hours. Then the AgCl precipitate was filtered off and to the supernatant 0.9 equivalent of 4-(4′-(1-adamantyl)phenyl)pyridine (0.14 mmol, 41 mg) was added and the reaction mixture was stirred for 24 hours at 60 °C. To the clear reaction mixture 10 mL of methanol was added. Then 30 mL of diethyl ether was added to precipitate the product. The white product that precipitated was filtered out and washed with 10 mL of diethyl ether. This procedure was repeated 3–5 times to remove all the residual DMF from the mixture and obtain the pure product.

2. Yield: 59%. ^{1}H NMR (700 MHz, DMSO-d_6): δ = 1.76 (d, 6H, CH_2), 1.90 (s, 6H, CH_2), 2.08 (s, 3H, CH), 4.17 (bs, 3H, NH_3), 4.56 (bs, 3H, NH_3), 7.55 (d, 2H, CH), 7.86 (d, 2H, CH), 7.91 (dd, 2H, CH), 8.71 (d, 2H, CH) ppm. ^{13}C NMR (700 MHz, DMSO-d_6): δ = 153.28 (C6), 123.33 (C7), 127.45 (C10), 126.4 (C11), 42.78 (C14), 28.67 (C15), 36.56 (C16). ESI-MS(+) *m*/*z* 554.1688 $[C_{21}H_{29}ClN_3Pt]^+$, calc. 554.1693.

*Synthesis of **3**.* To a solution of cisplatin (0.33 mmol, 100 mg) in 10 mL DMF, $AgNO_3$ (0.33 mmol, 55.7 mg) was added. The reaction mixture was stirred in the dark at 60 °C for 24 hours. Then the AgCl precipitate was filtered off and to the supernatant 0.9 equivalent of 4-phenylpyridine (0.29 mmol, 45 mg) was added and the reaction mixture was stirred for 24 hours at 60 °C. To the clear reaction mixture 10 mL of methanol was added. Then 30 mL of diethyl ether was added to precipitate the product. The white product that precipitated was filtered out and washed with more diethyl ether. This procedure was repeated 3–5 times to remove all the residual DMF from the mixture and obtain the pure product.

3. Yield: 55%. ^{1}H NMR (700 MHz, DMSO-d_6): δ = 4.36 (bs, 3H, NH_3), 4.66 (bs, 3H, NH_3), 7.58 (m, 3H, CH), 7.90 (dd, 2H, CH), 7.92 (m, 2H, CH), 8.78 (dd, 2H, CH) ppm. ^{13}C NMR (700 MHz, DMSO-d_6): δ = 152.96 (C6), 127.15 (C7), 135.11 (C8), 132.93 (C9), 123.15 (C10), 129.49 (C11), 130.54 (C12) ppm. ^{195}Pt NMR (700 MHz, D_2O): δ = −2297 ppm. ESI-MS(+) *m*/*z* 420.0586 $[C_{11}H_{15}ClN_3Pt]^+$, calc. 420.0588.

*Synthesis of **4**.* To a solution of cisplatin (0.16 mmol, 50 mg) in 10 mL DMF, $AgNO_3$ (0.16 mmol, 27 mg) was added. The reaction mixture was stirred in the dark at 60 °C for 24 hours. Then the AgCl precipitate was filtered off and to the supernatant 0.9 equivalent of 4-(pentafluorophenyl)pyridine (0.14 mmol, 34 mg) was added and the reaction mixture was stirred for 36 hours at 60 °C. To the clear reaction mixture 10 mL of methanol was added. Then 30 mL of diethyl ether was added to precipitate the product. The pale yellow product that precipitated was filtered out and washed with 10 mL of diethyl ether. This procedure was repeated 3–5 times to remove all the residual DMF from the mixture and obtain the pure product.

4. Yield: 44%. ^{1}H NMR (700 MHz, DMSO-d_6): δ = 4.35 (bs, 3H, NH_3), 4.68 (bs, 3H, NH_3), 7.79 (dd, 2H, CH), 8.92 (dd, 2H, CH) ppm. ^{13}C NMR (700 MHz, DMSO-d_6): δ = 154.28 (C6), 127.53 (C7), 144.07 (C10), 137.93 (C11), 141.91 (C12) ppm. ^{19}F NMR (300 MHz, DMSO-d_6): δ = −140.26 (d, 2F, CF), −150.20 (t, 1F, CF), −158.40 (t, 2F, CF) ppm. ^{195}Pt NMR (700 MHz, D_2O): δ = −2280 ppm. ESI-MS(+) *m*/*z* 510.0117 $[C_{11}H_{10}ClF_5N_3Pt]^+$, calc. 510.0113.

*Synthesis of **n_aq** (n = 1–4).* $AgNO_3$ (0.024 mmol, 4 mg) was added to a solution of *n* (0.024 mmol) in 3 mL of D_2O. The reaction mixture was stirred in the dark at 60 °C for 24 h, and the precipitated AgCl was filtered off. The filtrate contained the aqua form ***n*_aq**, in which chloride had been replaced by water. The filtrate was used for ^{1}H NMR measurements without further purification.

1_aq. ^{1}H NMR (700 MHz, D_2O): δ = 1.73 (d, 3H, CH_2), 1.67 (d, 3H, CH_2), 1.82 (s, 6H, CH_2), 2.01 (s, 3H, CH), 7.51 (d, 2H, CH), 8.50 (d, 2H, CH) ppm.

2_aq. ^{1}H NMR (700 MHz, D_2O): δ = 1.74 (d, 3H, CH_2), 1.69 (d, 3H, CH_2), 1.87 (s, 6H, CH_2), 2.02 (s, 3H, CH), 7.60 (d, 2H, CH), 7.77 (d, 2H, CH), 7.79 (d, 2H, CH), 8.64 (d, 2H, CH) ppm.

3_aq. ^{1}H NMR (700 MHz, D_2O): δ = 8.67 (d, 2H, CH), 7.81 (d, 2H, CH), 7.77 (m, 2H, CH), 7.51–7.54 (m, 3H, CH) ppm.

4_aq. ^{1}H NMR (700 MHz, D_2O): δ = 8.81 (d, 2H, CH), 7.70 (d, 2H, CH), −143.34 (dd, 2F, CF), −151.77 (t, 1F, CF), −161.81 (m, 2F, CF) ppm.

Theoretical methods

Unbiased molecular dynamics simulations. Parametrization and production simulation were all performed in the Amber 22 package.[55] All guest molecules were parametrized in the MCPB.py module[56] using the gaff2 force field. The same force field was also used in the antechamber package to parameterize the host molecule. The standard Langevin MD simulation was then performed with the total simulated of 2 μs. Trajectory analysis was performed with the help of the cpptraj program. For all snapshots, the oriented distance (ODIS) was calculated (see main text) and the resulting distributions were

Open Access Article. Published on 23 October 2024. Downloaded on 2/12/2026 1:15:43 AM. This article is licensed under a Creative Commons Attribution 3.0 Unported Licence.

fitted with the Gaussian mixture. A more detailed description of the whole procedure can be found in the ESI.†

Biased MD simulations. All ABF[57,58] simulations were performed in the PMFLib package.[59,60] Collective Variables (CVs) were selected to explore the free energy of dissociation of the HG complex. The oriented distance (ODIS) was used as the primary CV, with two additional helper CVs to aid in the sampling. The Multiple Walkers Approach[61] was employed to further enhance the sampling along the main CV and reduce the computational time. A more detailed description of the CVs used and the overall setup can be found in ESI.†

DFT calculations of secondary chemical shifts. The CB7 host and all guest geometries were optimized individually using the RI-B3LYP/def2TZVPP/COSMO(water) approach in Orca 5.0.[62] The obtained geometries were used to construct models of inclusion HG complexes differing in the ODIS coordinate of the guest molecule. Thirteen orientations of the guest in the equatorial plane were generated for each ODIS position. These collections of models were subjected to DFT calculations of the ^{1}H NMR shielding of the guest anchor (without geometry relaxation) – this procedure is referred to as "Rigid Scan" and was performed in Orca 5.0. Complexation-induced (secondary) NMR shifts were calculated relative to the free guest molecule. The final values of the complexation shifts were determined as the Boltzmann weighted average based on the free energy profile obtained from the ABF simulation.

Nuclear Independent Chemical Shifts (NICS) were calculated on the cubic grid (dimensions: 10 × 10 × 8.25 Å, voxel size 0.25 Å) of ghost atoms distributed in the cavity of CB7 and described at the same level of theory as in the case of the Rigid Scan. The geometries of the unbiased MD snapshots were projected into an NICS 3D map and the values of shielding obtained were averaged across the entire trajectory.

Evaluation of biological activity

Chemical and biochemical reagents. Cell culture medium RPMI-1640, mycoplasma-free fetal bovine serum (FBS), antibiotics penicillin–streptomycin, ethylenediaminetetraacetic acid (EDTA), trypsin, dimethyl sulfoxide (DMSO), and all other chemicals were purchased from Sigma-Aldrich Co., unless noted otherwise.

Cell cultures. In this study, two human ovarian cancer cell lines were used. The A2780 human ovarian cancer cell line, which is derived from the tumor tissue of an untreated patient, is frequently used as a model for assessing the impacts of various compounds. The A2780/CP cell line was established through chronic exposure of the parental cell line A2780 to cisplatin. Both cell lines used in this study were purchased from HPA Culture Collections (Salisbury, U.K.). Both cell lines were maintained in RPMI-1640 culture medium enriched with 10% FBS and supplemented with antibiotics (penicillin 100 units per mL and streptomycin 0.1 mg mL^{-1}). The cells were cultured in an incubator (Sanyo) at 37 °C in a humidified 5% CO_2 mixture with ambient air.

Measurement of cell viability. In this study, the cytotoxic effect of compounds **1**, **3**, **4**, reference cisplatin, and their HG complexes with CB7 and β-CD was determined using an MTT assay. A2780 and A2780/CP cancer cells were seeded into 96-well plates at a density of 8 × 10^3 cells per well, using 200 μL per well of RPMI-1640 culture medium supplemented with 10% FBS and 1% penicillin–streptomycin. Plates with cells were incubated at 37 °C in a humidified 5% CO_2 mixture. After 48 hours, the culture medium was removed and replaced with a 200 μL per well of fresh culture medium containing the test compound or its HG complex, with concentration ranging from 0 to 600 μM. Following 24 or 48 hours of exposure to the test compound, the culture medium with drugs was replaced with 200 μL per well of fresh culture medium containing 1 mg mL^{-1} MTT reagent. The plates were then kept in a humidified atmosphere at 37 °C for 4 h, wrapped in aluminum foil. After 4 hours, the medium containing MTT reagent was replaced with 200 μL of 99.9% DMSO per well to dissolve formazan crystals. Finally, the absorbance was read at a wavelength of 570 nm by a Cytation 3 Imaging multimode imaging reader from BioTek Instruments (Winooski, VT). All measurements were performed in quadruplicate. The IC_{50} values represent the concentration at which a substance demonstrates half of its maximum inhibitory impact.

Determination of platinum content in cell material and saturated aqueous solutions. Both cell lines were cultured in RPMI-1640 medium containing 10% FBS and 1% penicillin–streptomycin and incubated for 48 h in cell culture dishes (25 cm^2). Then, the cells were treated with 2.5 μM concentrations of compounds **1**, **3**, **4**, reference cisplatin, and their HG complexes with CB7 and β-CD, each at a sub-IC_{50} concentration. The purpose of using this concentration was to detect platinum accumulation without inducing cell death. Following incubation for 24 or 48 hours, the cells were harvested by trypsinization. The cells were washed three times with PBS, followed by centrifugation (4 °C, 2700 rpm, 7 minutes) to eliminate drugs bound to the cell surface. Subsequently, the cells were mechanically lysed in PBS on ice using a micropestle for 5 minutes, followed by centrifugation (4 °C, 2700 rpm, 7 minutes).

The platinum content of the cell supernatant after centrifugation was determined using a quadrupole ICP-MS spectrometer, specifically the Agilent 7900 (Agilent Technologies, Japan). Prepared lysates were diluted tenfold with Milli-Q water. The Pt concentration was measured by utilizing the isotope ^{195}Pt in reference to an internal standard (a solution of Au with a concentration of 1 μg L^{-1}) to suppress potential matrix effects and the instability of the plasma conditions. Quantification was carried out through external calibration within a range from 0.01 to 10 μg L^{-1} of Pt. The amount of platinum was expressed in μg L^{-1} and then converted to nanograms of Pt per 10^9 cells.

The relative solubilities of the Pt-compounds and their inclusion complexes studied were obtained by ICP-MS determination of the platinum concentration in saturated aqueous samples: the solutions were filtered and diluted 10^6-fold with Milli-Q water.

 This journal is © the Partner Organisations 2024

Open Access Article. Published on 23 October 2024. Downloaded on 2/12/2026 1:15:43 AM. This article is licensed under a Creative Commons Attribution 3.0 Unported Licence.

Author contributions

Conceptualization: J. N. and R. M.; methodology J. N., P. K., and R. M.; project administration: R. M.; experimental investigation: S. S. P., J. N., K. P., P. J., K. R., and M. K.; data curation: S. S. P., J. N., J. J., K. P., P. J., M. K., P. K.; writing – original draft: S. S. P., J. N., and R. M.; writing – review and editing: all authors; visualization: S. S. P., J. N., and J. J.; funding acquisition: M. M. and R. M.; resources: J. N., M. M., and R. M.; supervision: J. N., P. K., M. M., and R. M.

Data availability

The data that support the findings of this study are available in the ESI.† Crystallographic data for compound **3** have been deposited at the Cambridge Crystallographic Data Centre (CCDC no. 2371255†). The NMR spectra have been deposited at Mendeley Data and can be accessed *via* **https://doi.org/10.17632/7ymkxzbwjk.1**. The computational results are available in the ioChem-BD repository[63] and can be accessed *via* **https://doi.org/10.19061/iochem-bd-6-406**.

Conflicts of interest

There are no conflicts to declare.

Acknowledgements

This work has received support from the Czech Science Foundation (Grant No. 24-10760S to R. M.) and the Grant Agency of Masaryk University (MUNI/R/1568/2020 to M. K., MUNI/A/1575/2023, and MUNI/A/1587/2023). We acknowledge the Core Facilities NMR and X-ray of CIISB, Instruct-CZ Centre, supported by MEYS CR (LM2023042) and the European Regional Development Fund-Project "UP CIISB" (no. CZ.02.1.01/0.0/0.0/18_046/0015974). The computational resources were provided by the e-INFRA CZ project (ID: 90254, J. N.) supported by MEYS CR. The authors thank Sára Kollárová for the graphic design of the TOC.

References

1 B. Rosenberg, L. Van Camp and T. Krigas, Inhibition of Cell Division in Escherichia Coli by Electrolysis Products from a Platinum Electrode, *Nature*, 1965, **205**, 698–699, DOI: **10.1038/205698a0**.

2 R. C. Todd and S. J. Lippard, Inhibition of Transcription by Platinum Antitumor Compounds, *Metallomics*, 2009, **1**(4), 280–291, DOI: **10.1039/B907567D**.

3 R. Oun, Y. E. Moussa and N. J. Wheate, The Side Effects of Platinum-Based Chemotherapy Drugs: A Review for Chemists, *Dalton Trans.*, 2018, **47**(19), 6645–6653, DOI: **10.1039/C8DT00838H**.

4 D. M. Baguley and P. Prayuenyong, Looking beyond the Audiogram in Ototoxicity Associated with Platinum-Based Chemotherapy, *Cancer Chemother. Pharmacol.*, 2020, **85**(2), 245–250, DOI: **10.1007/s00280-019-04012-z**.

5 V. Stojanovska, S. Sakkal and K. Nurgali, Platinum-Based Chemotherapy: Gastrointestinal Immunomodulation and Enteric Nervous System Toxicity, *Am. J. Physiol.: Gastrointest. Liver Physiol.*, 2015, **308**(4), G223–G232, DOI: **10.1152/ajpgi.00212.2014**.

6 G. Daugaard and U. Abildgaard, Cisplatin Nephrotoxicity, *Cancer Chemother. Pharmacol.*, 1989, **25**(1), 1–9, DOI: **10.1007/BF00694330**.

7 E. Wong and C. M. Giandornenico, Current Status of Platinum-Based Antitumor Drugs, *Chem. Rev.*, 1999, **99**(9), 2451–2466, DOI: **10.1021/cr980420v**.

8 G. Damia and M. Broggini, Platinum Resistance in Ovarian Cancer: Role of DNA Repair, *Cancers*, 2019, **11**(1), 119, DOI: **10.3390/cancers11010119**.

9 D. J. Stewart, Mechanisms of Resistance to Cisplatin and Carboplatin, *Crit. Rev. Oncol. Hematol.*, 2007, **63**(1), 12–31, DOI: **10.1016/j.critrevonc.2007.02.001**.

10 E. Martinez-Balibrea, A. Martínez-Cardús, A. Ginés, V. Ruiz de Porras, C. Moutinho, L. Layos, J. L. Manzano, C. Bugés, S. Bystrup, M. Esteller and A. Abad, Tumor-Related Molecular Mechanisms of Oxaliplatin Resistance, *Mol. Cancer Ther.*, 2015, **14**(8), 1767–1776, DOI: **10.1158/1535-7163.MCT-14-0636**.

11 M. A. Skowron, C. Oing, F. Bremmer, P. Ströbel, M. J. Murray, N. Coleman, J. F. Amatruda, F. Honecker, C. Bokemeyer, P. Albers and D. Nettersheim, The Developmental Origin of Cancers Defines Basic Principles of Cisplatin Resistance, *Cancer Lett.*, 2021, **519**, 199–210, DOI: **10.1016/j.canlet.2021.07.037**.

12 I. Berger, A. A. Nazarov, C. G. Hartinger, M. Groessl, S.-M. Valiahdi, M. A. Jakupec and B. K. Keppler, A Glucose Derivative as Natural Alternative to the Cyclohexane-1,2-Diamine Ligand in the Anticancer Drug Oxaliplatin?, *ChemMedChem*, 2007, **2**(4), 505–514, DOI: **10.1002/cmdc.200600279**.

13 M. Trauner and J. L. Boyer, Bile Salt Transporters: Molecular Characterization, Function, and Regulation, *Physiol. Rev.*, 2003, **83**(2), 633–671, DOI: **10.1152/physrev.00027.2002**.

14 S. Jin, Y. Guo and X. Wang, Development of Platinum Complexes for Tumor Chemoimmunotherapy, *Chem. – Eur. J.*, 2024, **30**(10), e202302948, DOI: **10.1002/chem.202302948**.

15 S. Jin, E. Yin, C. Feng, Y. Sun, T. Yang, H. Yuan, Z. Guo and X. Wang, Regulating Tumor Glycometabolism and the Immune Microenvironment by Inhibiting Lactate Dehydrogenase with Platinum(IV) Complexes, *Chem. Sci.*, 2023, **14**(31), 8327–8337, DOI: **10.1039/D3SC01874A**.

16 Y. Wang, L. Cai, H. Li, H. Chen, T. Yang, Y. Tan, Z. Guo and X. Wang, Overcoming Cancer Resistance to Platinum Drugs by Inhibiting Cholesterol Metabolism, *Angew. Chem., Int. Ed.*, 2023, **62**(42), e202309043, DOI: **10.1002/anie.202309043**.

Open Access Article. Published on 23 October 2024. Downloaded on 2/12/2026 1:15:43 AM. This article is licensed under a Creative Commons Attribution 3.0 Unported Licence.

17 R. Canetta, M. Rozencweig and S. K. Carter, Carboplatin: The Clinical Spectrum to Date, *Cancer Treat. Rev.*, 1985, **12**, 125–136, DOI: 10.1016/0305-7372(85)90027-1.
18 E. Raymond, S. G. Chaney, A. Taamma and E. Cvitkovic, Oxaliplatin: A Review of Preclinical and Clinical Studies, *Ann. Oncol.*, 1998, **9**(10), 1053–1071, DOI: 10.1023/A:1008213732429.
19 T. C. Johnstone, K. Suntharalingam and S. J. Lippard, The Next Generation of Platinum Drugs: Targeted Pt(II) Agents, Nanoparticle Delivery, and Pt(IV) Prodrugs, *Chem. Rev.*, 2016, **116**(5), 3436–3486, DOI: 10.1021/acs.chemrev.5b00597.
20 S. Jin, Y. Guo, Z. Guo and X. Wang, Monofunctional Platinum(II) Anticancer Agents, *Pharmaceuticals*, 2021, **14**(2), 133, DOI: 10.3390/ph14020133.
21 T. C. Johnstone, G. Y. Park and S. J. Lippard, Understanding and Improving Platinum Anticancer Drugs – Phenanthriplatin, *Anticancer Res.*, 2014, **34**(1), 471–476.
22 T. C. Johnstone, J. J. Wilson and S. J. Lippard, Monofunctional and Higher-Valent Platinum Anticancer Agents, *Inorg. Chem.*, 2013, **52**(21), 12234–12249, DOI: 10.1021/ic400538c.
23 S. Zhang, K. S. Lovejoy, J. E. Shima, L. L. Lagpacan, Y. Shu, A. Lapuk, Y. Chen, T. Komori, J. W. Gray, X. Chen, S. J. Lippard and K. M. Giacomini, Organic Cation Transporters Are Determinants of Oxaliplatin Cytotoxicity, *Cancer Res.*, 2006, **66**(17), 8847–8857, DOI: 10.1158/0008-5472.CAN-06-0769.
24 K. S. Lovejoy, R. C. Todd, S. Zhang, M. S. Mccormick, J. Alejandro D'aquino, J. T. Reardon, A. Sancar, K. M. Giacomini and S. J. Lippard, Cis-Diammine(Pyridine) Chloroplatinum(II), a Monofunctional Platinum(II) Antitumor Agent: Uptake, Structure, Function, and Prospects, *Proc. Natl. Acad. Sci. U. S. A.*, 2008, **105**(26), 8902–8907, DOI: 10.1073/pnas.0803441105.
25 D. Wang, G. Zhu, X. Huang and S. J. Lippard, X-Ray Structure and, Mechanism of RNA Polymerase II Stalled at an Antineoplastic Monofunctional Platinum-DNA Adduct, *Proc. Natl. Acad. Sci. U. S. A.*, 2010, **107**(21), 9584–9589, DOI: 10.1073/pnas.1002565107.
26 G. Y. Park, J. J. Wilson, Y. Song and S. J. Lippard, Phenanthriplatin, a Monofunctional DNA-Binding Platinum Anticancer Drug Candidate with Unusual Potency and Cellular Activity Profile, *Proc. Natl. Acad. Sci. U. S. A.*, 2012, **109**(30), 11987–11992, DOI: 10.1073/pnas.1207670109.
27 N. J. Wheate, S. Walker, G. E. Craig and R. Oun, The Status of Platinum Anticancer Drugs in the Clinic and in Clinical Trials, *Dalton Trans.*, 2010, **39**(35), 8113–8127, DOI: 10.1039/C0DT00292E.
28 X. Wang and Z. Guo, Targeting and Delivery of Platinum-Based Anticancer Drugs, *Chem. Soc. Rev.*, 2013, **42**(1), 202–224, DOI: 10.1039/C2CS35259A.
29 S. Dilruba and G. V. Kalayda, Platinum-Based Drugs: Past, Present and Future, *Cancer Chemother. Pharmacol.*, 2016, **77**(6), 1103–1124, DOI: 10.1007/s00280-016-2976-z.
30 H. Yin, Q. Cheng, D. Bardelang and R. Wang, Challenges and Opportunities of Functionalized Cucurbiturils for Biomedical Applications, *JACS Au*, 2023, **3**(9), 2356–2377, DOI: 10.1021/jacsau.3c00273.
31 N. Saleh, A. L. Koner and W. M. Nau, Activation and Stabilization of Drugs by Supramolecular pK_a Shifts: Drug-Delivery Applications Tailored for Cucurbiturils, *Angew. Chem., Int. Ed.*, 2008, **47**(29), 5398–5401, DOI: 10.1002/anie.200801054.
32 N. J. Wheate, Improving Platinum(II)-Based Anticancer Drug Delivery Using Cucurbit[n]Urils, *J. Inorg. Biochem.*, 2008, **102**(12), 2060–2066, DOI: 10.1016/j.jinorgbio.2008.06.005.
33 S. Shukla, B. Sagar, A. K. Sood, A. Gaur, S. Batra and S. Gulati, Supramolecular Chemotherapy with Cucurbit[n]Urils as Encapsulating Hosts, *ACS Appl. Bio Mater.*, 2023, **6**(6), 2089–2101, DOI: 10.1021/acsabm.3c00244.
34 W. Jogadi and Y.-R. Zheng, Supramolecular Platinum Complexes for Cancer Therapy, *Curr. Opin. Chem. Biol.*, 2023, **73**, 102276, DOI: 10.1016/j.cbpa.2023.102276.
35 Y. J. Jeon, S.-Y. Kim, Y. H. Ko, S. Sakamoto, K. Yamaguchi and K. Kim, Novel Molecular Drug Carrier: Encapsulation of Oxaliplatin in Cucurbit[7]Uril and Its Effects on Stability and Reactivity of the Drug, *Org. Biomol. Chem.*, 2005, **3**(11), 2122–2125, DOI: 10.1039/B504487A.
36 L. Cao, G. Hettiarachchi, V. Briken and L. Isaacs, Cucurbit[7]Uril Containers for Targeted Delivery of Oxaliplatin to Cancer Cells, *Angew. Chem., Int. Ed.*, 2013, **52**(46), 12033–12037, DOI: 10.1002/anie.201305061.
37 B. Z. Momeni and A. S. Abd-El-Aziz, Recent Advances in the Design and Applications of Platinum-Based Supramolecular Architectures and Macromolecules, *Coord. Chem. Rev.*, 2023, **486**, 215113, DOI: 10.1016/j.ccr.2023.215113.
38 W.-C. Geng, J. L. Sessler and D.-S. Guo, Supramolecular Prodrugs Based on Host–Guest Interactions, *Chem. Soc. Rev.*, 2020, **49**(8), 2303–2315, DOI: 10.1039/C9CS00622B.
39 M. Sojka, J. Chyba, S. S. Paul, K. Wawrocka, K. Hönigova, B. J. R. Cuyacot, A. C. Castro, T. Vaculovič, J. Marek, M. Repisky, M. Masařik, J. Novotny and R. Marek, Supramolecular Coronation of Platinum(II) Complexes by Macrocycles: Structure, Relativistic DFT Calculations, and Biological Effects, *Inorg. Chem.*, 2021, **60**(23), 17911–17925, DOI: 10.1021/acs.inorgchem.1c02467.
40 S. J. Barrow, S. Kasera, M. J. Rowland, J. Del Barrio and O. A. Scherman, Cucurbituril-Based Molecular Recognition, *Chem. Rev.*, 2015, **115**(22), 12320–12406, DOI: 10.1021/acs.chemrev.5b00341.
41 K. I. Assaf and W. M. Nau, Cucurbiturils as Fluorophilic Receptors, *Supramol. Chem.*, 2014, **26**(9), 657–669, DOI: 10.1080/10610278.2014.929130.
42 D. Veclani, A. Melchior, M. Tolazzi and J. P. Cerón-Carrasco, Using Theory To Reinterpret the Kinetics of Monofunctional Platinum Anticancer Drugs: Stacking Matters, *J. Am. Chem. Soc.*, 2018, **140**(43), 14024–14027, DOI: 10.1021/jacs.8b07875.

This journal is © the Partner Organisations 2024

Open Access Article. Published on 23 October 2024. Downloaded on 2/12/2026 1:15:43 AM. This article is licensed under a Creative Commons Attribution 3.0 Unported Licence.

43 Z. Deng, H. Yao, Z. Wang and G. Zhu, Platinum Anticancer Drugs: Targeting and Delivery, in *Comprehensive Inorganic Chemistry III (Third Edition)*, ed. J. Reedijk and K. R. Poeppelmeier, Elsevier, Oxford, 2023, ch. 2.25, pp. 808–846. DOI: 10.1016/B978-0-12-823144-9.00130-8.

44 J. J. Wilson and S. J. Lippard, Synthetic Methods for the Preparation of Platinum Anticancer Complexes, *Chem. Rev.*, 2014, **114**(8), 4470–4495, DOI: 10.1021/cr4004314.

45 S. Dasari and P. Bernard Tchounwou, Cisplatin, in Cancer Therapy: Molecular Mechanisms of Action, *Eur. J. Pharmacol.*, 2014, **740**, 364–378, DOI: 10.1016/j.ejphar.2014.07.025.

46 W. M. Nau, M. Florea and K. I. Assaf, Deep Inside Cucurbiturils: Physical Properties and Volumes of Their Inner Cavity Determine the Hydrophobic Driving Force for Host–Guest Complexation, *Isr. J. Chem.*, 2011, **51**(5–6), 559–577, DOI: 10.1002/ijch.201100044.

47 C. W. Fong, Cisplatin Cyclodextrin Complexes as Potential Free Radical Chemoradiosensitizers for Enhanced Cisplatin Treatment of Cancers: A Quantum Mechanical Study, *J. Inclusion Phenom. Macrocyclic Chem.*, 2017, **89**(3), 343–351, DOI: 10.1007/s10847-017-0760-2.

48 S. Liu, C. Ruspic, P. Mukhopadhyay, S. Chakrabarti, P. Y. Zavalij and L. Isaacs, The Cucurbit[n]Uril Family: Prime Components for Self-Sorting Systems, *J. Am. Chem. Soc.*, 2005, **127**(45), 15959–15967, DOI: 10.1021/ja055013x.

49 K. S. Lovejoy, M. Serova, I. Bieche, S. Emami, M. D'Incalci, M. Broggini, E. Erba, C. Gespach, E. Cvitkovic, S. Faivre, E. Raymond and S. J. Lippard, Spectrum of Cellular Responses to Pyriplatin, a Monofunctional Cationic Antineoplastic Platinum(II) Compound, in Human Cancer Cells, *Mol. Cancer Ther.*, 2011, **10**(9), 1709–1719, DOI: 10.1158/1535-7163.MCT-11-0250.

50 J. A. Plumb, B. Venugopal, R. Oun, N. Gomez-Roman, Y. Kawazoe, N. S. Venkataramanan and N. J. Wheate, Cucurbit[7]Uril Encapsulated Cisplatin Overcomes Cisplatin Resistance via a Pharmacokinetic Effect, *Metallomics*, 2012, **4**(6), 561–567, DOI: 10.1039/C2MT20054F.

51 L. Amable, Cisplatin Resistance and Opportunities for Precision Medicine, *Pharmacol. Res.*, 2016, **106**, 27–36, DOI: 10.1016/j.phrs.2016.01.001.

52 G. R. Fulmer, A. J. M. Miller, N. H. Sherden, H. E. Gottlieb, A. Nudelman, B. M. Stoltz, J. E. Bercaw and K. I. Goldberg, NMR Chemical Shifts of Trace Impurities: Common Laboratory Solvents, Organics, and Gases in Deuterated Solvents Relevant to the Organometallic Chemist, *Organometallics*, 2010, **29**(9), 2176–2179, DOI: 10.1021/om100106e.

53 G. M. Sheldrick, SHELXT – Integrated Space-Group and Crystal-Structure Determination, *Acta Crystallogr., Sect. A: Found. Adv.*, 2015, **71**(1), 3–8, DOI: 10.1107/S2053273314026370.

54 G. M. Sheldrick, Crystal Structure Refinement with SHELXL, *Acta Crystallogr., Sect. C: Struct. Chem.*, 2015, **71**(1), 3–8, DOI: 10.1107/S2053229614024218.

55 D. A. Case, H. M. Aktulga, K. Belfon, D. S. Cerutti, G. A. Cisneros, V. W. D. Cruzeiro, N. Forouzesh, T. J. Giese, A. W. Götz, H. Gohlke, S. Izadi, K. Kasavajhala, M. C. Kaymak, E. King, T. Kurtzman, T.-S. Lee, P. Li, J. Liu, T. Luchko, R. Luo, M. Manathunga, M. R. Machado, H. M. Nguyen, K. A. O'Hearn, A. V. Onufriev, F. Pan, S. Pantano, R. Qi, A. Rahnamoun, A. Risheh, S. Schott-Verdugo, A. Shajan, J. Swails, J. Wang, H. Wei, X. Wu, Y. Wu, S. Zhang, S. Zhao, Q. Zhu, T. E. I. Cheatham, D. R. Roe, A. Roitberg, C. Simmerling, D. M. York, M. C. Nagan and K. M. Merz Jr., AmberTools, *J. Chem. Inf. Model.*, 2023, **63**(20), 6183–6191, DOI: 10.1021/acs.jcim.3c01153.

56 P. Li and K. M. Merz Jr., MCPB.Py: A Python Based Metal Center Parameter Builder, *J. Chem. Inf. Model.*, 2016, **56**(4), 599–604, DOI: 10.1021/acs.jcim.5b00674.

57 E. Darve, D. Rodríguez-Gómez and A. Pohorille, Adaptive Biasing Force Method for Scalar and Vector Free Energy Calculations, *J. Chem. Phys.*, 2008, **128**(14), 144120, DOI: 10.1063/1.2829861.

58 J. Comer, J. C. Gumbart, J. Hénin, T. Lelièvre, A. Pohorille and C. Chipot, The Adaptive Biasing Force Method: Everything You Always Wanted To Know but Were Afraid To Ask, *J. Phys. Chem. B*, 2015, **119**(3), 1129–1151, DOI: 10.1021/jp506633n.

59 PMFLib, https://pmflib.ncbr.muni.cz/, accessed 2023-12-22.

60 T. Bouchal, I. Durník, V. Illík, K. Réblová and P. Kulhánek, Importance of Base-Pair Opening for Mismatch Recognition, *Nucleic Acids Res.*, 2020, **48**(20), 11322–11334, DOI: 10.1093/nar/gkaa896.

61 K. Minoukadeh, C. Chipot and T. Lelièvre, Potential of Mean Force Calculations: A Multiple-Walker Adaptive Biasing Force Approach, *J. Chem. Theory Comput.*, 2010, **6**(4), 1008–1017, DOI: 10.1021/ct900524t.

62 F. Neese, The ORCA Program System, *Wiley Interdiscip. Rev.: Comput. Mol. Sci.*, 2012, **2**(1), 73–78, DOI: 10.1002/wcms.81.

63 M. Álvarez-Moreno, C. de Graaf, N. López, F. Maseras, J. M. Poblet and C. Bo, Managing the Computational Chemistry Big Data Problem: The ioChem-BD Platform, *J. Chem. Inf. Model.*, 2015, **55**(1), 95–103, DOI: 10.1021/ci500593j.